MINISTRY OF EDUCATION AND TRAINING

VIETNAM ACADEMY OF SCIENCE AND TECHNOLOGY

GRADUATE UNIVERSITY OF SCIENCE AND TECHNOLOGY

Dang Thi Le Hang

INJECTABLE ALGINATE AND PLURONIC-BASED HYDROGELS WITH ON-DEMAND BIOACTIVE COMPOUNDS FOR SPECIFIC TISSUE REGENERATION

SUMMARY OF DISSERTATION

ON ORGANIC CHEMISTRY

Code: 9 44 01 14

Ho Chi Minh City- 2024

The dissertation is completed at: Graduate University of Science and Technology, Vietnam Academy Science and Technology

Supervisors:

Tran Ngoc Quyen, Associated Professor, Institute of Applied Material and Sience

Referee 1: ....

Referee 2: ....

Referee 3: ....

The dissertation will be examined by Examination Board of Graduate University of Science and Technology, Vietnam Academy of Science and Technology at……………………….. (time, date……)

The dissertation can be found at:

1. Graduate University of Science and Technology Library
2. National Library of Vietnam

CHAPTER 1 : INTRODUCTION

1.1   Motivation of study: the importance of thermal-responsive hydrogel in tissue engineering and the current challenge

Millions of deaths occur globally each year due to injuries and diseases that cause tissue damage, with a profound impact on the quality of life and a substantial healthcare burden [1-4]. Despite the introduction of organ transplantation, conventional reconstruction may be unsuitable in many cases [5, 6]. Allografts face limitations such as the availability of appropriate human grafts, necessity for immunosuppression, and technical challenges [7, 8]. Immunosuppressive measures for graft recipients carry significant risks, including susceptibility to infections, elevated risk of cancer, and reduced life expectancy [6, 8]. In response to these challenges, there has been a rapid development in studies in the field of tissue regeneration [1, 3, 5]. The primary objective of these studies had been to create functional human tissue equivalents for organ repair and replacement [9, 10].

A fundamental concept in tissue regeneration involves the use of biomaterials that mimic the structure of the extracellular matrix (ECM) to support new cell growth and promote repair [1, 5, 10]. While decellularized techniques initially provided ideal biomaterials (dECM) for tissue regeneration [4, 11-14], concerns regarding relevance, ethical approval, scaling-up, and cost have prompted a shift towards the use of safe and effective tissue-engineered scaffold alternatives [2, 3, 10]. Among these, hydrogels have emerged as prominent and versatile materials for tissue regeneration [1, 3, 5]. Hydrogels are characterized by highly hydrated three-dimensional (3D) networks of water-soluble polymers [1, 3]. Their swollen and hydrated structures closely resemble the ECM in the native tissues, creating a microenvironment favorable for regenerated cells [15, 16]. The porous structure of the hydrogels supported the encapsulation process. It can act as cargo for sensitive biological cues, making it an excellent choice for carrying and releasing drugs/ therapeutic agents [2, 3, 16]. The soft features of hydrogels can help reduce the inflammatory response of the surrounding tissue, thereby enhancing its biocompatibility [1, 15]. Hydrogels can easily adjust their shape according to private requirements, making them preferred for implantable materials and devices [2, 10].

In recent years, injectable hydrogels have gained more attention than conventional gels because of their advantages in minimally-invasive surgical procedures and real-time adaptability in shape [17, 18]. Injectable gels are essentially a type of in situ forming hydrogel that simplifies cargo incorporation, making them preferable delivery vehicles [19]. This hydrogel form is particularly suitable for applications in which the final form or shape is either unimportant or defined by the void or space into which they are injected [17, 18]. Apart from the in situ gelling characteristic, the term "injectable" implies that the hydrogel is created through a process that primarily involves the transport of the sol or prequel to a targeted site for gelation via an injection device [15, 17]. The need for injectable hydrogels has spurred the use of smart hydrogels that exhibit structural responses to temperature changes [17, 19-21]. In such hydrogels, at a critical gelation concentration (CGT), the hydrogel displays the behavior of the fluid, transforming from a sol to a gel state above that temperature [17, 22]. Polymers with a low critical solution temperature or phase transition between room temperature and body temperature have been employed to create injectable in situ hydrogels [17]. After injection into the body, the polymer solution underwent thermally induced self-assembly to form a hydrogel at body temperature [20]. A significant focus has been the development of thermosensitive hydrogels by combining thermo-responsive polymers with natural polymeric components, such as polysaccharides[20, 23]. This combination allows for rational design of artificial environments conducive to cell growth and differentiation [24]. Polysaccharides, either conjugated with a thermosensitive polymer or cross-linked with a combination of both polysaccharide and thermosensitive polymers, have been utilized to prepare thermally responsive hydrogels with an optimal critical solution temperature suitable for injection into the body [20, 22, 23]. This combination also offers new possibilities for developing suitable mechanical strengths for each tissue application [15, 16].

Combining all the essential features of a pure hydrogel form often makes it challenging to fulfill the fundamental requirements for the desired clinical application. The recognition of the limitations of hydrogels has led to the development of hybrid systems with different biological cues [25, 26]. By incorporating bioactive compounds such as amino acids [27-29], plant-derived bioactive substances [30-32], and/or bioglass [27, 33] into hydrogels, these systems acquire characteristics that the bare form of the scaffold cannot achieve on their own. Interestingly, strengthening hydrogels through biophysical factors may outperform or replace the effects of biochemical cues [34], particularly in applications where such factors effectively encourage cultured and/or recruited cells to form functional tissues [29, 31, 32]. Therefore, there is a compelling need to explore the application of innovative synthetic designs to address these challenges and create materials that offer greater programmability.

1.2 Aims and object

This project aimed to identify and develop innovative injectable scaffolds with thermally responsive properties and on-demand requirements for tissue regeneration. This was achieved using hybrid polymer material, specifically polysaccharide, alginate, and the thermal-responsive polymer Pluronic F127. The objective was to create scaffolds that provided a well-defined and suitable microenvironment for guiding cells predictably, thus facilitating tissue regeneration. In addition, a delicate combination of biological cues (plant-driven compound-resveratrol, amino acids (arginine), or inorganic nanoparticles (bioglass) would be expected as singling regulators in the designed hydrogel systems to enhance and promote the synergetic efficacy of these materials in tissue regeneration.

Two broad approaches are commonly used to design thermally responsive hydrogels from Pluronic F127 and alginate: grafting and crosslinking. Therefore, this thesis has two main objectives:

The project aims 1: To develop a thermally responsive hydrogel from alginate and Pluronic F127 via grafting techniques. The hypothesis is that after Pluronic grafting on alginate, the sol-gel transition feature will remain, while the pore structure will support cell development. The designed structure would be a scaffold for dual therapeutic agents to assist in diabetic wound treatment.

The project aims 2: To develop a thermally responsive hydrogel by employing crosslinking techniques on a combination of alginate and Pluronic F127, utilizing catechol oxidative crosslinking for bone regeneration. Bioglass could be introduced to develop biomimetic functional hydrogels for bone regeneration. To eliminate the peroxidase enzyme's use for the catechol oxidative reaction, the bioglass was engineered with hemin nanoparticles to introduce a new function to the bioglass system. The hypothesis is that the peroxidase-mimicking enzyme based on bioglass acts as a catalyst to facilitate catechol oxidation, resulting in the formation of crosslinking in alginate and Pluronic with suitable sol-gel transition. The addition of bioglass could also provide a potential scaffold for bone regeneration.

1.3 Structure of a thesis

The thesis has six chapters. The first chapter is the introduction (3 pages), the second chapter is a literature review (37 pages), and the third chapter is the methodology (17 pages). The result and discussion section are divided into 2 chapters: Chapter 4 (objective 1, 37 pages) and Chapter 5 (objective 2, 27 pages). Finally, the conclusion, limitation, and recommendations segment are presented in Chapter 6 (4 pages). Some results are presented in the appendix. The thesis integrates 9 tables, 41 figures, and 2 schematics. It includes 311 references, with 187 from the past 5 years, representing 60.13%.

CHAPTER 2   STATE OF THE ART AND LITERATURE REVIEW

2.1 The concept of injectable thermal responsive hydrogel in tissue regeneration

2.2 Encoding the hydrogel for specific tissue regeneration

2.2.1 The stiffness of the hydrogel

2.2.2 The biological cues

2.2.2.1 Diabetic wound

2.2.2.2 Bone regeneration

2.3 Pluronic derived thermal responsive hydrogel-forming materials

2.4 Alginate- A versatile material for regenerative medicine applications

CHAPTER 3 : MATERIALS AND EXPERIMENTAL METHODS

All the materials, reagents, and analyzed equipment were presented in the main text.

3.1 Synthesis of polymer

3.1.1 Preparation of Pluronic precursor

3.1.1.1 Preparation of the Pluronic-NPC,

This procedure was based on previous reports [71-72]. The hydroxyl group in Pluronic F127 was activated by p-nitrophenyl chloroformate (pNPC), resulting in a carbonate derivative (strong electrophile), which is easy to form a covalent bond with nucleophile functional groups such as amino NH_2.

3.1.1.2 Preparation of Pluronic-DOPA (PDA)

The pluronic-dopamine (PDA) derivative was synthesized with the help of p-NPC. After activating pluronic F127 with pNPC, the carbamate linkages were formed between the carbonates group in pluronic-NPC and amino groups in DOPA.

3.1.2 Preparation of alginate precursor

3.1.2.1 Preparation of alginate-cystamine

The derivative alginate-cystamine (AC) was synthesised with the help of EDC (1-ethyl-3-(3-dimethylaminopropyl)carbodiimide), NHS (N-hydroxysuccinimide). The carboxylate groups on alginate were activated with EDC to form the strong electrophile O-acylisourea, which easily formed the chemical bond with nucleophilic NH_2 on cystamine molecular. NHS was used along with EDC to increase the stability of O-acylisourea derivative alginate.

3.1.2.2 Preparation of alginate-DOPA

The derivative alginate-DOPA (ADA) was synthesized with the help of EDC (1-ethyl-3-(3-dimethylaminopropyl)carbodiimide). The carboxylate groups on alginate were activated with EDC to form the strong electrophile O-acylisourea, which easily formed the chemical bond with nucleophilic NH_2 on cystamine molecular.

3.1.3 Preparation of alginate-cystamine –Pluronic

Alginate-cystamine-pluronic (ACP) was the result of the carbamate linkage between pluronic-NPC and NH_2 group on the derivative alginate-cystamine.

3.1.4 Characterization technique for the resultant structure

The chemical structure of the products was verified using Fourier transform infrared spectroscopy, proton nuclear resonance, and UV-vis (UV-1900, Shimadzu, Japan). The density of amino groups on the alginate was determined by 2,4,6-trinitrobenzene sulfonic acid (TNBS, Thermo Fisher Scientific) using l-alanine as an internal standard. The substitution degree of DOPA on alginate or Pluronic was calculated using the monitoring absorbance at 280 nm.

3.2 Preparation of peroxidase mimicking bioglass

3.2.1 Preparation of HNP

HNP nanoparticles were prepared from hemin by hydrothermal method in methanol.

3.2.2 Preparation of HNP BG

Bioactive glass was prepared by sol-gel method, with the formula of 64% SiO_2–31% CaO–5% P_2O_5 (in mol %). HNP nanoparticles were merged in the network of bioglass by hydrothermal method as similar procedure at section 3.2.1.

3.2.3 Structure characterization

Morphology was identified by scanning electron microscopes (SEM, JSM IT-200 Jeol) equipment with energy dispersive spectrometry (EDS) to analyze the element distribution. X-ray diffraction was performed with D8 Advance ECO (Bruker AXS, Germany) to identify the crystallization of products. The UV–vis absorption spectra were recorded in a UV–vis spectrophotometer (UV-1900, Shimadzu, Japan). Fluorescence spectra were recorded by Fluoromax Plus C (Horiba, Japan).

3.3 **Peroxidase-like activity test**

3.3.1 Pyrogallol assay

Pyrogaollol assay was conducted to identify the ability to mimic the catalyst function of peroxidase. HRP enzyme was used as a reference. Based on the kinetic of the oxidative reaction of pyrogallol, the Km and Vmax of HNP BG values were calculated and then compared with those induced by the HPR enzyme in the same condition. This assay was performed with UV-vis (UV-1900, Shimadzu, Japan).

3.3.2 Oxidative dopamine reaction

The oxidative reaction of dopamine (DOPA) was used to evaluate the mimicking reactions of peroxidase in the preparation of polydopamine. HRP enzyme was used as a reference. This assay was performed with UV-vis (UV-1900, Shimadzu, Japan). UHPLC Ultimate 3000 – MSQ Plus analyzed the formation of polydopamine.

3.4 **Preparation of hydrogel**

3.4.1 Preparation of hydrogel from alginate-cystamine-Pluronic ACP

The ACP powder was dissolved in DI water at different concentrations (0-20 wt%) and stirred at 10–15 °C. The aqueous solution was stable at 4°C for 24h before forming gel at room temperature.

3.4.2 Preparation of dopamine crosslinking hydrogel

Solution A: The derivative Pluronic-DOPA (PDA) was dissolved in DI water and stirred at 10–15 °C. The aqueous solution was stable at 4°C for 24h. The concentration of PDA for making gel was investigated from 20 wt%.

Solution B: The derivative alginate-DOPA (ADA) was dissolved in DI water and stirred at room temperature.

Solution A was mixed with H_2O_2 for PDA hydrogel before adding HNP BG. The concentration of PDA in combination with HNP BG to make hydrogel was investigated based on the study of hydrogel from solution A without oxidative agents and catalysts.

For the PDA-ADA hydrogel, solutions A and B were mixed, and the concentration of A was selected based on the study about the formation of PDA hydrogel with H_2O_2 and HNP BG. The concentration of ADA varied from 0.1 to 2 wt%.

3.5 **Characterization of the morphology of the resultant hydrogels**

The dry morphology was done by SEM. Hydrogel at the wet stage was studied with a confocal microscope with the help of AO as a dye.

3.6 **Thermal responsive testing**

3.6.1 Test tube inversion method

The CGC and GT values of the design materials were evaluated using the test tube inversion method, which involves transferring polymer solution to the tube at the tested temperature and concentration.

3.6.2 *Rheological analysis*

Rheology was studied with Thermo HAAKE 6000 or TA Discovery HR 30.

3.7 **Water uptake and degradation test**

The ability of hydrogel in water uptake and degradation were performed with DMEM, PBS $1\times$, and DI water. The water uptake ability was investigated via the change in mass of hydrogel as the function of time after soaking in selected media. The degradation of hydrogel was calculated via the change of the mass of copolymer before and after soaking.

3.8 **Drug encapsulation and in vitro release study**

3.9 **Drug encapsulation**

The encapsulated process was performed using the ball milling method [266].

3.9.1 *Released test*

The release of biological cues was tested via dialysis with a 3.5kDa cellulose membrane. The amount of release was analyzed using HPLC in combination with ELSD. The kinetic drug release was recorded using KinetDS 3.0 open-source software.

3.10 **Cell Cytotoxic test**

3.10.1 *Cytotoxic test with 2D culture*

The hydrogel extract was used in this test. SRB assay was conducted to evaluate the viability of the cell after contacting the extract solution.

3.10.2 *Cytotoxic test with 3D cell culture*

Cells were mixed with a copolymer to form a hydrogel. A live/dead staining assay, AO/PI, characterized cell toxicity.

3.10.3 *The function of cell-laden hydrogel*

The ability of a cell to move and become adhesive on a culture dish after culturing inside a hydrogel was used to test the function of cell-laden hydrogel and investigated via fluorescent dye.

3.11 **Anti-bacteria assay**

The anti-bacterial test was performed using diffusion disk and micro-dilution tests.

3.12 **Anti-oxidant test**

3.12.1 *DPPH assay*

DPPH assay was evaluated via the absorption of OD 517nm.

3.12.2 *Superoxide anion assay*

The superoxide anion ($O^{2\bullet-}$) assay was tested via the amount of $O^{2\bullet-}$ produced in macrophage-like cells Raw 264.7 cells after activating by LPS by cytochrome c reductase kit.

3.12.3 *Monitoring the oxidative stress with BMSC cells*

This experiment was done with the oxidative stress cell. Indeed, BMSC cell was induced oxidative stress by H_2O_2. The, these cell was treated with the tested samples to investigate their effectiveness in recover after stress. These value was identified via the concentration of nitric oxide (with Griess assay) and the presence of peroxynitrite (with the flouresent marker J2™ PON Green 99).

3.13 **Hemolysis assay**

The hemolysis assay was used to test the blood compatibility feature of hydrogel. If the hydrogel induce the hemolysis greater than 10%, it would be concluded as toxic.

3.14 Biominimization assay

3.14.1 Biomineralization process in SBF

The hydrogel was incubated in SBF for the determined time. Then, it was collected and lyophilized. SEM with EDS was used to evaluate the formation of mineralized products on the surface of the hydrogel. XRD was included to analyze the formation of crystals on the surface of the hydrogel after soaking.

3.14.2 Osteoinductive assay

The assay was done with hMSCs cells. After incubating the cells with the tested sample, the accumulation of calcium via Alizarin Red dye was used to investigate the differentiated process of stem cells hMSCs.

3.15 Animal study

The animal studies were conducted at the University of Science, Nam National University, Ho Chi Minh City, and Ho Chi Minh Medicine University.

Albino mice (CD-1 ICR, Coat Color White—Albino) and white rabbits from New Zealand were involved in this research, which was supported by the Institute of Drug Quality Control Ho Chi Minh City.

3.15.1 Skin irritation test

The protocol was established with the guidance of ISO 10993-10:2010 (E).

3.15.2 Toxicology studies

The toxicity of hydrogel was tested with a subcutaneous injection performed at Ho Chi Minh Medicine University (ethical number: 958/GCN-HĐĐĐNCTĐV signed date 16/6/2023). After the injection, the parameters of white blood cell components and the C-reactive protein (CRP) were analyzed to identify the inflammation. The skin at the injected site was evaluated by histology hematoxylin-eosin (HE).

3.15.3 Establishing the diabetic mice model with STZ

The diabetic mice were established with Streptozotocin (STZ), performed at the University of Science, Nam National University, Ho Chi Minh City (ethical number: 79B/KHTN-ACUCUS signed date 30/06/2020). STZ was single-injected via intravenous administration. The STZ dose was identified via the survival analysis Kaplan-Meier (KM) and the blood glucose concentration (measured via Accu Chek Performa). The STZ dose that induced blood glucose higher than 250 mg/dL during 14 days with a survival rate higher than 90% was selected for the wound healing test.

3.15.4 Establishing the burn wound model on diabetic mice

The burn wound model on diabetic mice was made by a heated metal rod with a diameter of 0.5 cm. The wound was treated after two days of induced burn. The samples were injected with a 25G needle with a dose of 0.4mL/ wound. The wound was treated every two days.

3.15.5 Evaluation of wound healing process

The closure process of the wound was recorded every 2 days. The wound was measured with a caliper. The wound area was estimated following the previous protocol [71, 72]. The histology was done with H&E and Masson's trichrome (MT). These studies were done in the Pathology Department- University of Medicine and Pharmacy at Ho Chi Minh City, Vietnam. The re-epithelization was estimated based on the thickness of the epidermal layer with the help of the AxioVision 3.0 program. The estimation of the collagen fraction was done using ImageJ software.

3.16 Data analysis

OrginPro2022B and Graph-Pad Primes 2021 were used to calculate and present the results. All data was collected from 3 replications. The significant difference was concluded if the p-value was lower than 0.05.

CHAPTER 4 CONSTRUCTION OF THERMAL RESPONSIVE HYDROGEL FROM ALGINATE AND PLURONIC VIA GRAFT TECHNIQUES FOR DIABETIC WOUND HEALING

4.1   Characterization of alginate-pluronic copolymerization

Pluronic F127 was grafted on the alginate backbone via the cystamine as a bridge, presented in **Figure 4.1**. Cystamine was first introduced on the alginate via the help of EDC/NHS, resulting in the amine-functionalized alginate, donated as Alginate-cystamine (AC). To graft pluronic on Na-alg-cys at the amino group, the hydroxyl terrminal group of pluronic was activated with p-nitrophenyl chloroformate (NPC) to form p-nitrophenyl carbonate, donated as NPC-F127. The p-nitrophenyl carbonate group on NPC-F127 is very reactive towards the amino group of AC by means of stable urethane linkages. Thus, the reaction between NPC-F127 and Na-alg-cys occurred in water at RT condition. The chemical structure was analyzed with FT-IR, 1H-NMR, and UV-vis.
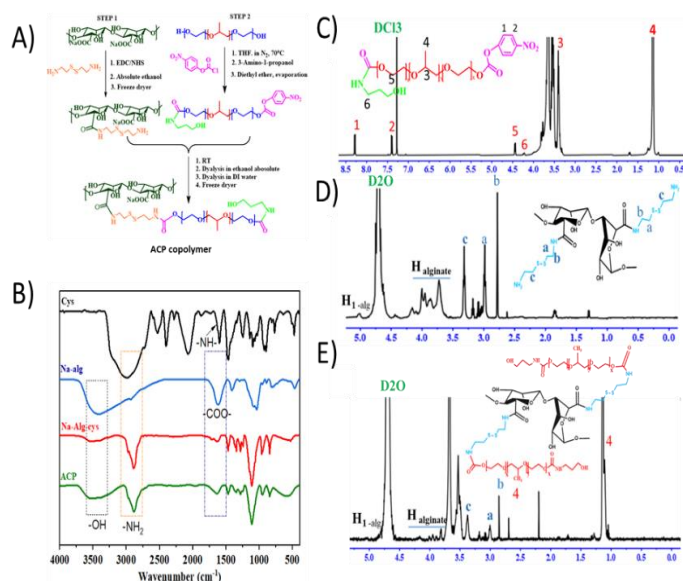

Figure 4.1: *A) Schematic for grafting approached design of copolymerization from Alginate and pluronic F127. B) FT-IR spectra of precursor polymers and resultant polymer. 1H-NMR spectra of precursor pluronic (C), precursor alginate (D), and ACP copolymer (E).*

4.1.1   Characterization of the precursor alginate, alginate-cystamine

For alginate-cystamine (AC), the carboxyl groups on the Na-alg backbone were activated to form O-acylurea that could react quickly with primary amines [56]. FT-IR was conducted to evaluate the modified carboxylic group on the Na-alg process (**Fig 4.1B**). The FT-IR spectrum of Na-Alg: 3411 cm^{-1} for hydroxyl groups (-OH), 2923 cm^{-1} for aliphatic (CH$_2$), 1619 cm^{-1} and 1412 cm^{-1} for symmetric and asymmetric stretching (-COO-), respectively[57]. 1294–815cm^{-1}, some vibrations for ether functional groups (C-O-C) in glycosidic linkage[58]. The vibration peaks in 890-815 cm^{-1} belong to the C-C and C-O bond in mannuronic acid [59], while the exhibition of the pyranoid ring in guluronic acid is characterized at 1294cm^{-1}-1037cm^{-1} [57]. After modification with cystamine, the major characterizations of Na-alg (O-H, C=O) are still presented in FT-IR spectra of AC. However, the blue shift is observed for symmetric and asymmetric carboxyl groups compared to the pure Na-Alg, suggesting the interaction of amine groups on carboxylic groups [60]. The spectrum shows the additional peak with strong absorption at 2890 cm^{-1} assigned to the vibration of primary amine, along with a small signal of SH bonding at 2298-1960 cm^{-1}. Notably, the anomeric peak of the fingerprint at 1700 cm^{-1} and 1243 cm^{-1} shows the characteristic absorption bands of N-C=O (amine I) and N-H bending vibrations, proposing the amidation of the carboxylic group of alginate molecules.[61] The success of aminated functional Na-alg was further confirmed via ^{1}H-NMR spectra in **Figure 4.1D**. Both the characteristic proton peaks of Na-alg and cystamine are presented in the ^{1}H-NMR spectra. The spectra display the anomeric proton on the guluronic unit (H1-G) and mannuronic unit (H1-M) at δ =5.05ppm and

δ = 4.45ppm [62,63], respectively. These spectra also show the chemical shift corresponding to proton C-5 of the guluronic unit (H5-G, at δ= 4.37ppm) and mannuronic unit (H5-M, δ=4.20ppm)[64]. In addition, the spectrum exhibits these signals at δ= 3.1 ppm (Ha) and δ= 3.4 ppm (Hb) arising from the respective proton of -CH$_2$CH$_2$S- and -NHCH$_2$CH$_2$S-, which help to confirm the success of derivative alginate-cystamine [65]. Throughout the TNBS assay, the coupled amine content is 54.70±0.36 mg/g of AC, yielding 78.04±2.31%.

4.1.2   *Characterization of the precursor pluronic, pluronic –NPC*

The hydroxyl groups on the pluronic F127 backbone were first activated with p-NPC, and its chemical characterization was presented in **Figure 4.1C**. This spectrum shows a chemical shift for the protons of the aromatic ring of p-NPC at δ = 7.41 ppm (H2) and δ = 8.29 ppm (H1). The proton signals of PPO blocks of Pluronic F127 are at δ =1.15 ppm (H4, methyl group(-CH$_3$)) and δ =3.41ppm (H3, methylene group (>CH$_2$), whereas the proton –CH$_2$ −CH$_2$– units of PEO blocks is at δ = 3.67 ppm. In addition, the chemical shift at δ = 4.44 ppm (H5) is assigned to the proton on the methylene group in the ester bond with p-NPC, CH$_2$-O-NPC. Also, the peak at δ = 4.22ppm corresponds to methylene protons of CH$_2$−CH$_2$–O-Ami moiety, confirming the success of the second route.

4.1.3   *Characterization of alginate-pluronic copolymerization*

The successful synthesis of ACP was also confirmed by FT-IR and ^{1}H-NMR spectra (**Fig 4.1**). ACP copolymer exposes all typical characteristic peaks in the FT-IR spectrum of Na-alg-cys. The introduction of pluronic on the AC backbone induces the changing intensity of the stretching of ester groups (C=O) and hydroxyl groups (OH). The proof of a covalent chemical bond between pluronic and AC is the presence of the deformation vibrations of NH bonds and stretching vibrations of CN in the FT-IR spectrum of ACP copolymer. ^{1}H-NMR was used to confirm this result further). ^{1}H NMR (**Fig. 4.1E**) confirmed the successful synthesis of the ACP grafted copolymer (600 MHz, d-H$_2$O): pluronic F127 (δ=1.04 ppm for CH$_3$ (1) on PPO block, δ=3.702 ppm for CH$_2$ (2) on PEO block)[10,66]; alginate (δ=5.02 ppm (H1), 4.46 ppm, 4.39 ppm for guluronic acid proton, δ=4.43, 3.91 ppm for manuronic acid proton)[10]; cystamine (δ=2.99 ppm (a), 3.37 ppm (c) for methylene (–CH$_2$))[67]. Regarding the remaining amine content calculated by TNBS assay, the grafting reaction efficiency of the activated pluronic was about 44.47±0.74%.

4.2   **Preparation of the thermal-sensitive hydrogel from alginate-pluronic copolymerization**

4.2.1   *The effect of alginate on the thermal sensitive property of the resultant hydrogel*

Cohesive energy density is a term in rheology that measures the strength of a material's internal structure [68,69]. The coherent energy of pluronic F127 was improved after grafting to the alginate backbone. The cohesive energy density of the pluronic F127 solution (20 %wt) at 35°C was 28.8 Pa. After grafting on the alginate backbone (APC with pluronic accounting for 87.5% by mass), the cohesive energy was 1655 times improved. However, when the feed ratio of alginate increased (APC with pluronic accounting for 83.33% by mass), the coherent energy density was reduced. It was 158.84 Pa, about 300 times reduction compared to APC from 87.5% pluronic.

Also, it was found that viscoelastic parameters of ACP are mainly determined by the content of pluronic F127 in grafting samples (**Fig 4.2A-B**). When the feed content of pluronic F127 is 83.33%, the LVE region exists at deficient shear strain, under 2% for 45°C and 4% for 35°C. It was observed that ACP copolymer solution at this ratio showed viscoelastic liquid behavior at 35°C, suggesting that this solution could not form a gel stage at a temperature below 37 ^{o}C even though its copolymer concentration was up to 20 %wt as seen in **Fig. 4.2A**. A marginal shift in the LVE region was observed when the mass fraction of pluronic F127 increased to 87.5%. The LVE region was 3.8% at 35°C and 8.4% at 10°C. In addition, with 87.5% pluronic F127 in the grafting reaction (fig 4.2B), the values of the loss modulus G' were more significant than the value of store modulus G' at 35°C, confirming that at the beginning of the test, the superstructure formed a consistent, three-dimensional network[70]. These results agreed with cohesive energy density. To better understand alginate's effect, the critical gel

concentration of pure pluronic F127 was determined. The sol-gel transition of pluronic F127 at 20 wt% was at 20.01°C. This gel critical temperature (GCT) was shifted to a higher point with the incorporation of alginate. For example, with ACP from 83.33% pluronic, the GCT was at 44.89°C, while ACP from 87.5% pluronic set up their GCT at 35.1 °C. The GCT values depended on the amount of pluronic F127. An increase in alginate concentration makes the system more hydrophilic due to the nature of alginate[39,71]. The higher amount of alginate increases the density of hydrogen bonds with water molecules and then increases the enthalpy of dehydration[13,72,73]. The presence of alginate hinders both the initial structural rearrangement of micelles and the subsequent caging to form a packed, ordered gel structure[72,73]; consequently, it increases the gelation of the temperature. Because only ACP with 87.7% pluronic expressed the gel within the range of 30-37°C, this grafted copolymer was used for further study.
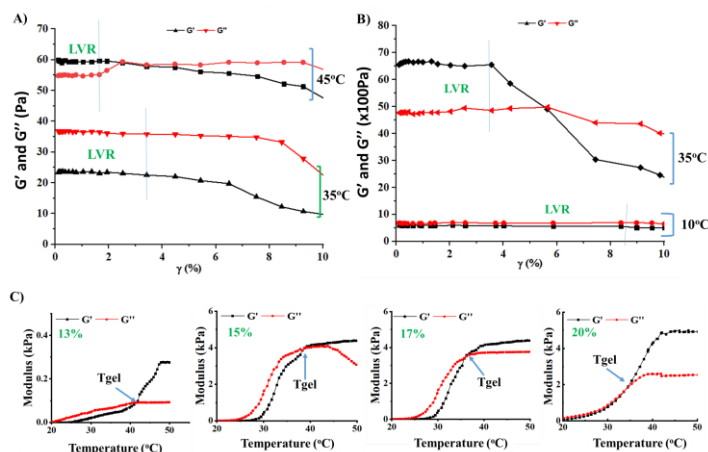

Figure 4.2*: The viscoelastic parameters of two ACP copolymers (20wt%)at difference pluronic contain, 83.33% (A) and 87.5% (B), as a function of strain amplitude at a fixed angular frequency of 1.0 rad/s in difference temperature conditions. C) Evolution of the dynamic moduli in temperature sweep experiment of ACP with various concentrations. A) 13 %wt, B) 15 %wt, C) 17 %wt and D) 20 %wt.*

4.2.2   The influence of the concentration of copolymer on the sol-gel transition of hydrogel

The thermal behavior of ACP copolymer through a sol-gel transition following the temperature function was tested and displayed in **Figure 4.2C**. The sol-gel transition of the ACP copolymer solution was strongly dependent on the concentration of ACP. When the copolymer concentration increased from 13% to 20% %wt, the temperature-induced Tgel was reduced. Specifically, at 13 %wt, the crossing point is at 41.2 °C, while it is reduced to 35.1 °C at 20 %wt. Moreover, the maximum value of G′ followed the order of concentrations, attributed to the decrease of copolymer ACP flexibility at higher concentrations[72,73]. Increasing ACP concentration leads to a higher density of hydrophobic interaction, thus resulting in a higher capacity to build the microstructure. Furthermore, the pluronic behavior in response to the change in temperature induces the folding of the alginate backbone, creating a more hydrophobic zone [74,75]. Similar to the jamming-induced gelation in pure Pluronic systems, the thermal gelation in the ACP system could be due to the pacing of micelles within the alginate folding pocket[75]. Subsequently, it potentially stores the deformation energy and reduces the isotropic gel[76]. Therefore, the higher concentration of ACP required lower heat energy to introduce the aggregation of ACP, consequently achieving lower Tgel.

4.2.3   The influence of the physiological solvent on the sol-gel transition of hydrogel

Next, besides the influence of concentration on Tgel, the effect of the aqueous media dissolved ACP copolymer on sol-gel transition temperature was investigated. As shown in **Figure 4.3A**, at 20 %wt of the copolymer, ACP dissolved in DI water, PBS buffer, or DMEM media undergoes the sol-gel transition in response to the heating condition. Regarding rheology, the solvent causes slight variations in Tgel values of ACP (**Fig 4.3C**). During heating, ACP dispersed in DI water (20 %wt) undergoes the sol-gel transition at 35.1°C. However, when

physiological buffer (PBS 7.4) or culture medium (DMEM) was used to prepare ACP hydrogel (20 %wt), the gelation occurred at a lower temperature than that of DI water. This may be due to the interaction of Na-alg with ions in the medium[60,65,77,78]. When the ACP polymer is dissolved in this solvent, the cationic ions diffuse into ACP networks, forming the ionic inter-chain bridges[73]. Therefore, the lower Tgel induced by the medium can be explained by the synergistic effect between the Pluronic copolymers and sodium alginate chains. Due to cationic agents in buffer media, the water surrounding the Pluronic chain may be reduced with the increase in temperature[79], and the PPO segments become more hydrophobic and less polar[80], providing a platform for promoting gelation. ACP hydrogel (20 %wt) could be a suitable scaffold for cell encapsulation processes in the concentration range and all solvents tested.
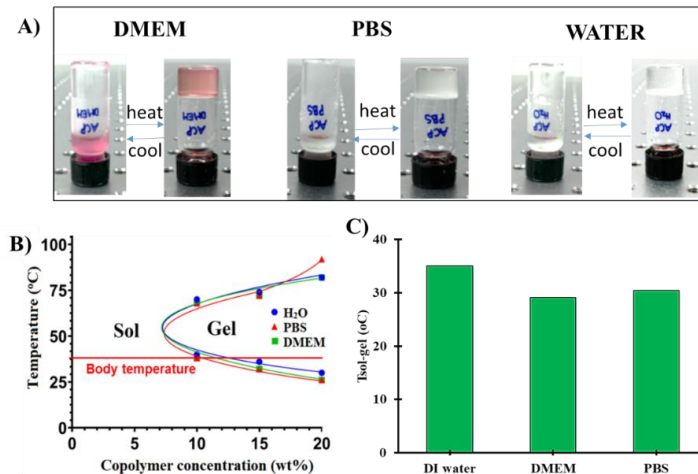

Figure 4.3: *A) Optical images of ACP copolymer (20 %wt) prepared in different solvents (DI water, DMEM, and PBS) when put at 2 different temperature conditions, below 20°C and above 30°C. B) The sol-gel transition temperature of the ACP hydrogels was prepared in different solvents (DI water, DMEM, and PBS) using the inverted tube method. C) Temperature-induced point, Tgel, identifying by rheology.*

4.3 Evaluation of cell-laden thermal responsive ACP hydrogel
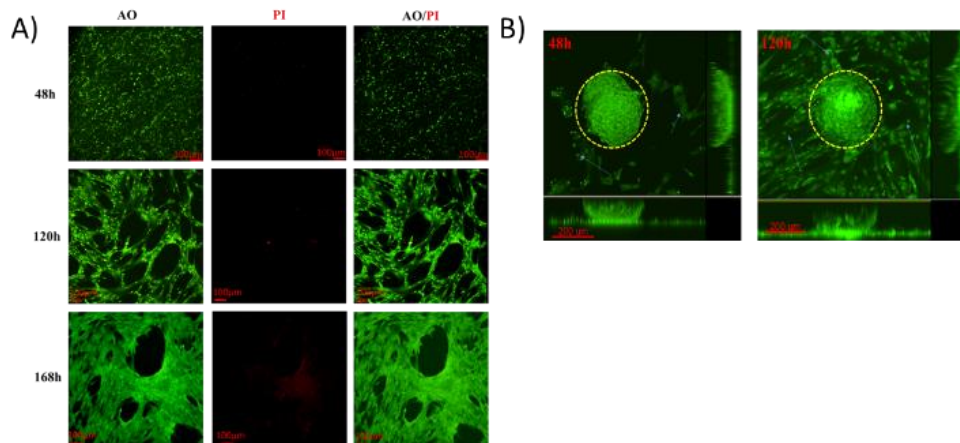
Figure 4.4: *A) Human fibroblast encapsulated in ACP hydrogel at 48 hr, 120 hr, and 168 hr. Cells were treated with dual AO/PI. Scale bar: 100µm. B) Z-stack fluorescence images of dual AO/PI staining of cells migrating out of encapsulated hydrogel droplet (20µl). A squared dot circle presented the formation of the ACP cluster, and blue arrows were used to identify the outgrowth cell from the ACP hydrogel. The ability of the resultant hydrogel in dual active compound incorporation toward the diabetic wound healing*

Fibroblast cells were encapsulated inside the ACP hydrogel matrix to prove the well-designed tissue-specific scaffolding template. After 48h culture, the viabilities of fibroblast cells were around 96.7 ± 3.5%, estimated by the number of green cells over red cells. For long-term culture, above 90% of fibroblast cells were

primarily stained green, demonstrating that most cells are viable. In other words, this indicates that the cells were grown in good culture conditions. After 24 hr incubation, BJ cells adhered to the wall of ACP hydrogel, proliferated, and extended within the ACP scaffolds after 120 hr. The growth of fibroblast cells increased rapidly and created a layered network saturating the hydrogel matrix after 168 hr (**Fig 4.4 A**). Furthermore, the morphology of fibroblast cells culturing inside ACP hydrogel was elongated, which is rarely seen under 3D culture conditions[81]. The elongation of fibroblast culturing inside hydrogel has been reported with a hydrogel system forming with biological cues such as alginate hydrogel modified with RGD peptide [82] or a hydrogel system forming with ECM derivative materials such as gelatin[83] or collagen[84]. In this study, the number of elongated fibroblast cells shown at 120 hr and 168 hr was higher than the established 3D hydrogel in those studies, confirming that ACP hydrogel mimicked the ECM structure. Next, the outgrowth cells released from ACP clusters seemed to develop the natural morphology of fibroblast cells (**Fig 4.4B**). Further, the outgrowth cells established the confluent cell layer on the surface of the culture dish at the 5th-day culture. This observation could confirm that the ACP scaffolds provided a favorable microenvironment for cell adhesion, spreading, and proliferation. Therefore, ACP hydrogel might be applied for tissue regeneration[85].

4.3.1 *Optimization of the concentration of L-arginine and resveratrol*

The single loading system was first developed to identify the concentration of biological cues (L-arginine and resveratrol) that should be encapsulated in the hydrogel. With resveratrol, a hydrophobic compound, the maximum amount of resveratrol loaded in hydrogel was investigated first. The maximum loading capacity of ACP hydrogel to Resveratrol was 22.12 ± 1.26 % (221.2 µg resveratrol per 1 mg ACP). ACP hydrogel with a maximum concentration of Resveratrol was non-toxic to fibroblast cells. In addition, the addition of Resveratrol was intolerant to the sol-gel transition temperature of ACP hydrogel. Therefore, ACP hydrogel was designed with Resveratrol at 50 and 100µg/mg of ACP polymer as R10-ACP and R20-ACP hydrogel, respectively. Various amounts of L-arginine (50-200 µg/mL) had been manufactured for the L-arginine loading system. However, A-ACP hydrogel induces cytotoxic effects on fibroblast cells in a dose-dependent manner. The density and morphology of the fibroblast cells cultured on ACP hydrogel with L- arginine concentration of 50 µg/mL or 100 µg/mL were almost identical to the control sample. When the L-arginine concentration in ACP hydrogel was increased to 150 µg/mL, fibroblast cells showed characteristic changes in morphology, similar to the senescence morphology of fibroblast cells induced by oxidative stress [278]. In addition, a massive apoptotic signal was observed. The shrunken and rounded cells with significant cytotoxicity were detected on ACP hydrogel with the highest concentration of L-arginine (200 µg/mL). In addition, adding A-ACP hydrogel showed the change in the pH value of culture media as the function of L-arginine. The pH value was 7.2 -7.4 when the L-arginine concentration in ACP was 50 µg/mL or 100 µg/mL. The higher alkaline environment (pH > 8.0) was recorded with ACP hydrogel containing 150 µg/mL or more. It is well-known the impact of the pH environment of dressing on the wound healing process [279, 280]. The alkaline environments decelerate cell migration, causing prolonged healing time, especially on the wound of hard-to-heal wounds such as diabetic wounds [279]. From the preliminary investigation, the arginine concentration in all hydrogel dressings was 100µg/ml. Based on these obtained results, the dual systems were set up with AR 10-ACP (resveratrol: 50 µg/mg ACP copolymer, L-arginine: 100µg/ml) and AR20- ACP (resveratrol: 100 µg/mg ACP copolymer, L-arginine: 100µg/ml).

4.3.2 *Characterization of thermal behavior of AR-ACP hydrogel*

In term of thermal gelling behavior, AR10-ACP hydrogel and AR20- ACP hydrogel showed sol-gel transition when the temperature surpassed 30°C and conversion to flowable sol upon cooling (Fig. 4.5A). This result was also authenticated by rheological behavior (**Fig 4.5B**). However, the biological cues expressed the impact on the rheological property of ACP hydrogel. The incorporation of Resveratrol reduced the critical sol-gel transition temperature. The gel–sol transition was shifted from 34.83 °C (**Fig 4.12B**) to 31.97°C when the amount

of Resveratrol in ACP was 50 µg/mg. This pattern was clearly confirmed with ACP hydrogel containing a higher amount of Resveratrol. In addition, the storage modulus was drastically increased following the incorporation of Resveratrol as similar as hydrogel encapsulating hydrophobic molecules [29, 72, 281]. Increased storage moduli in the liquid phase and reduced gelation temperatures as Resveratrol concentration rises imply a possible decrease in the distance between the clusters of the aggregated PPO segments due to the multiple hydrophobic sites [72, 281]. In contrast, the incorporation of L-arginine induced a higher gelation temperature. L-arginine is a hydrophilic and positively-charged amino acid [166, 282, 283]. L-arginine causes the electrostatic interaction with the carboxylate group on alginate in the ACP copolymer. The reduction in elastic moduli confirmed that the ionic strength was strong enough to suppress temperature-dependent solubility of PPO in water [281]. Therefore, a higher temperature was required for the sol-gel transition. Intriguingly, the modeling behavior of ACP hydrogel in a dual-loading system was adjusted by L-arginine and Resveratrol. The gelation temperature R10-ACP was increased from 31.97 °C to 34.04 °C following the support of L-arginine. For relatively higher Resveratrol, R20-ACP, these phenomena were similar. In other words, in the presentation of Resveratrol, the PPO segments might be manageable to close-packed to overlap the hydrophilic density [72]. Adding hydrophobic Resveratrol might reduce the influence of the electrostatic interaction between alginate and L-arginine. The thermogelling behavior of A-ACP hydrogel was decreased in the suitable application.
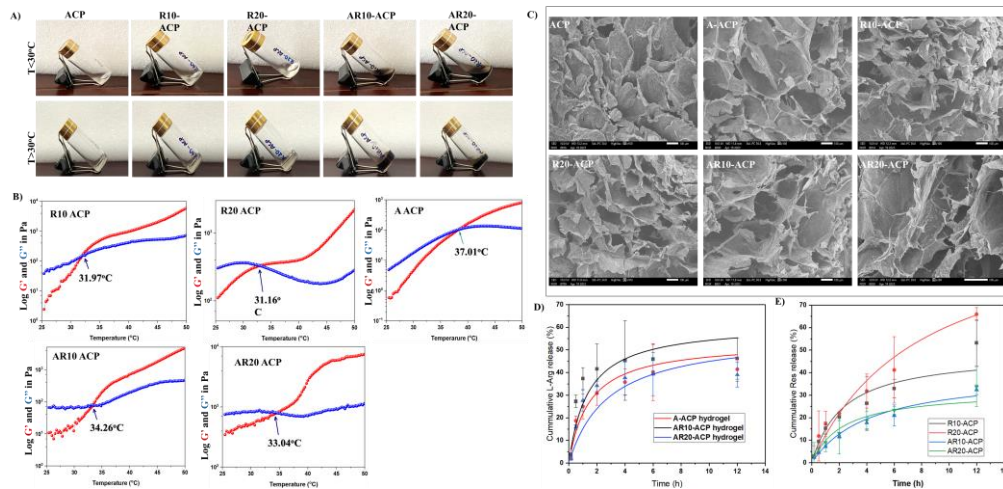
Figure 4.5: *A) Photographs showing reversible sol-gel transition behavior of ACP hydrogel with different loading agents in ACP hydrogel and its rheological study under oscillation temperature ramp (strain =1% and frequency = 10rad/s): B) A-ACP hydrogel; C) R10- ACP hydrogel; D) R20 - ACP hydrogel; E) AR10 – ACP hydrogel; F) AR20 – ACP hydrogel. The morphology of this hydrogel was obtained by SEM techniques with magnification = 100, SED = 10KeV (A). The release profiles of arginine (B) and resveratrol (C) from ACP hydrogel were monitored during the first 12 hours. Data was presented as mean ± SD (n=4).*

The porous structure of the ACP hydrogel was maintained despite adding different loading agents (**Fig 4.5C**). Due to the difference in properties of arginine and Resveratrol, the interconnected compact morphology with different pores was observed. With the addition of L-arginine, some of the fibril bundles are exposed in the interpenetrating channel, revealing the ionic coordination bonds between the alginate backbone and L-arginine. In the case of Resveratrol, the internal arrangements of the ACP network remained; however, there was a more compact porous structure than that of the pure one. This may result from the addition of the hydrophobic intermolecular fashion of Resveratrol and the hydrophobic zone of the ACP hydrogel network, consequently causing the tighter cross-linking between these micelles.

4.3.3   *Evaluation of release process of biological cues*

Table 4.1 :The kinetic release

Release kinetic model	Biological cues		Arginine			Resveratrol			
	Sample		A-ACP	AR10-ACP	AR20-ACP	R10-ACP	R20-ACP	AR10-ACP	AR20-ACP
Zero Order	R^2		0,37	0,57	0,45	0,95	0,96	0,99	0,95
First Order	R^2		0,23	0,31	0,28	0,62	0,59	0,72	0,73
KP*	R^2		0,67	0,76	0,74	0,96	0,94	0,99	0,99
	K		n/a	n/a	n/a	11,66	13,03	7,200	8,907
	n		0,49	0,58	0,66	0,67	0,68	0,62	0,54
Higuchi	R^2		n/a	0,62	0,49	0,90	0,88	0,93	0,99
Hixson-Crowell	R^2		0,27	0,39	0,33	0,76	0,7617	0,82	0,82
Modified KP*	R^2		0,98	0,99	0,98	0,92	0,94	0,79	0,79
	n		0,23	0,26	0,24	0,47	0,48	0,61	0,53
	t_{lag}		0,15	0,15	0,15	0,13	0,14	0,002	0,003
	K		32,57	24,67	24,307	15,19	18,09	7,22	8,94

*KP: Korsmeyer-Peppas; n/a: non observation.

The release profiles of both arginine and resveratrol were extensively investigated (**Fig. 4.5D-E**). The kinetic released models for drug release from the polymeric matrix [90,91], such as zero order, first order, Higuchi, Hixson-Crowell, Korsmeyer-Peppas, and its modified form with time lag, were presented in **Table 4.1**. Both arginine and resveratrol had a comparatively rapid release in the first 2 h and then showed a sustained release. As shown in **Table A1,** the modified Korsmeyer-Peppas has a more significant potential to be employed as a predictive model for Arginine from ACP hydrogel. Of note, L-arginine is a hydrophilic molecule. L-arginine molecules are preferred to be located at or near the hydrogel surface. Therefore, about 30-40% of arginine was leaked from the ACP system during 2 hours of immersion. Similarly, the arginine from the dual loading system, modified by Korsmeyer-Peppas, outperformed all exanimated models. The use of resveratrol along with L- arginine did not influence on the initial release time (tlag for A-ACP, AR10-ACP, and AR20-ACP were 0.23 h, 0.26 h, and 0.24 h, respectively). The diffusional exponent n was below 0.45 in all cases, confirming the L-arginine release mechanism's similarity. Interestingly, the kinetic coefficient k value was much lower for arginine from the dual system than the single system, confirming the influence of resveratrol in decelerating L-arginine release. By

comparing the Akaike Information Criterion (AIC) value, Zero-order and Korsmeyer-Peppas models were the preferred for the resveratrol system. Because all the diffusional exponent n for R10- ACP and R20- ACP were in the range 0.43−0.85, the release of resveratrol was influenced by diffusion and swollen matrix [90]. The drug release models to describe resveratrol release behavior from dual loading systems, AR10-ACP and AR20-ACP, were similar to R10-ACP and R20-ACP hydrogel. Also, the diffusional exponent suggested that resveratrol release from various dual systems relies on non-Fickian diffusion (0.43<n<0.85) [91]. However, the transport constants (K) were much higher for a single resveratrol loading system than resveratrol from a dual system. This phenomenon was similar to the release of L-arginine from a dual system. For the R-ACP system, the density of the hydrophobic zone in the ACP hydrogel increased following the encapsulation of resveratrol [10]. After immersion in a release buffer, water diffused into the network, causing the hydration of these zones; consequently, resveratrol could easily escape [71]. The support of L-arginine in the microstructure might provide more of a cage for resveratrol. Therefore, the release profiles of resveratrol in the dual system have been adjusted suitably.

4.3.4 The synergic of L-arginine and resveratrol dual loading ACP hydrogel in anti-oxidation activity

4.3.4.1 L-arginine controls the scavenging rate of resveratrol in a manner way.

The 1,1-diphenyl-2-picrylhydrazine (DPPH) radical assay was first carried out to estimate the antioxidant properties of hydrogels from the adsorption peak of 517 nm, and the results were presented in **Figure 4.6 A-B**. Due to the participation of sulphhydryl molecules in the ACP copolymer structure, which are effective free radical scavengers [92,93], the resultant ACP hydrogels exhibited promising antioxidant capacity. Many studies demonstrate the importance of radical agents in wound healing [128-129]. On the one hand, a low amount of radical agents aid in the defense of wounds against microbial infections and promote vascularization by activating multiple cellular signaling pathways [127]. On the other hand, the extensive production of ROS in diabetic patients impedes the wound healing process by blocking the normal physiological metabolism [94-97]. If radical detoxification is not performed at the appropriate time, the wound frequently becomes non-healing and chronic, making treatment challenging [10-21]. It was found that the addition of resveratrol or L-arginine displayed more remarkable scavenging capacity than those native ACP hydrogels (**Fig. 4.6A-B**). The combination of L-arginine and resveratrol provided an effective radical detoxifying strategy suitably. With single resveratrol, extreme scavenging activity was observed at 8h. With the addition of L-arginine, the scavemeyer rate was nearly two orders of magnitude lower than that of the single system (p= 0.00248, R10-ACP vs AR10-ACP; p=0.00493, R20-ACP vs AR20-ACP). The effective scavenging activity of AR-ACP hydrogel and R-ACP hydrogel was comparable after 96h of incubation (p=0.11688, R10-ACP vs AR10-ACP; p=0.62544, R20-ACP vs AR20-ACP).

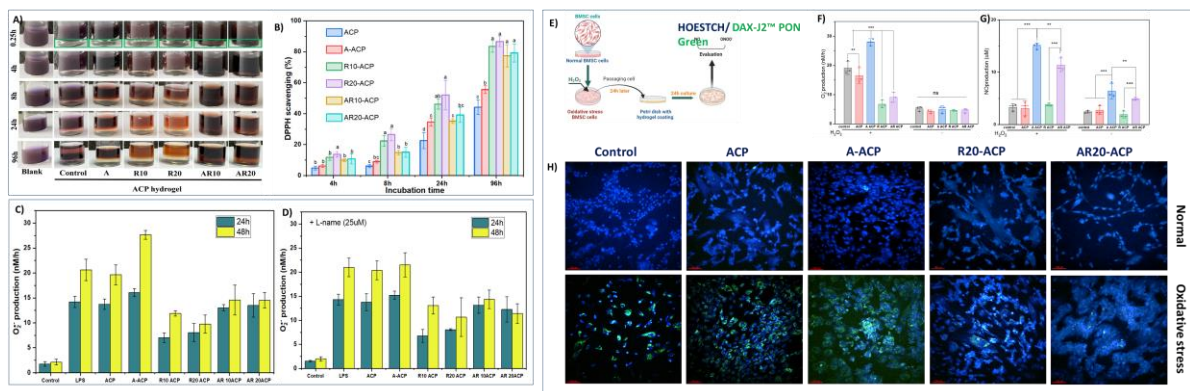**Figure 4.6**: A) Photographs of DPPH (0.5 mM) were added to various ACP hydrogels at different time points (green box indicated hydrogel layer). B) Compared to non-treated samples, The percentage of free DPPH radical scavenged by ACP hydrogels. Superoxide anion ($O^{2\bullet-}$) production in RAW 264.7 cells treated with ACP hydrogels in two-time points: 24h and 48h without C) L-name (NOS inhibitors) and D) with L-Name. Effect of AR-

*ACP hydrogel on the oxidative stress cells model of H_2O_2-induced oxidative. E) The illustration of the cell model. The concentration of $O^{2\cdot-}$ (F) and NO release (G) from normal and oxidative stress cells with different treatments after 24h culture (n = 3 individual experiments). (H)The cells stained with DAX-J2 PON (Green) to peroxynitrite (ONOO−) and Hoestch (Blue) to Nucleus. Data are expressed as mean ± SEM. Significant differences were detected by one-way ANOVA with Tukey's multiple comparisons test, *p<0.05, **p<0.01, ***p<0.001. ACP blank (control), A (A-ACP), R10 (R10-ACP), R20 (R20-ACP), AR10 (AR10-ACP), AR20 (AR20-ACP).*

4.3.4.2 Resveratrol prevents the generation of $O^{2\cdot-}$ production in the active immune cells.

$O^{2\cdot-}$ is the first ROS produced by macrophages upon contact with various activating stimuli (e.g., LPS, cytokines, growth factors, and fragments of bacterial membranes)[94,96,98]. Therefore, to verify whether the designed hydrogel could have the ability to eliminate intracellular ROS activity, the consumption of $O^{2\cdot-}$ production in stimulated Raw 264.7 cells was performed. The $O^{2\cdot-}$ formation was very high in the stimulated macrophage cells (**Fig. 4.6C**). After 24h of LPS stimulation, macrophages produced relatively high amounts of $O^{2\cdot-}$ production (14.2 ±1.1nM/h), about 8 times higher than that of unstimulated cells (p<0.05), which then increased up to 20.6 ±2.2nM/h at 48h (p<0.01). The effect of the native ACP hydrogel on the production of $O^{2\cdot-}$ could be ignored due to indistinguishable values compared to control LPS. At the same time, other ACP samples induced strong effects on the synthesis of this radical. There was a massive increase in $O^{2\cdot-}$ production in the stimulated cells incubated with A-ACP hydrogel, from 16.1±0.8 nM/h at 24h to 27.7±0.9nM/h at 48h, relative to 134.3% in LPS-stimulated cells (p<0.05). In contrast, ACP hydrogel with resveratrol leads to a marked reduction of $O^{2\cdot-}$ production. The concentration of $O^{2\cdot-}$ in both R10-ACP hydrogel and R20-ACP hydrogel was halved over A-ACP hydrogel (p<0.05) or stimulated cells (p<0.05) after 24h. Interestingly, the longer culture time did not seem to affect the level of $O^{2\cdot-}$ in the case of ACP hydrogel supplemented with resveratrol (p>0.05). Presumably, as an effect of resveratrol, dual AR-ACP hydrogels suppressed the amount of $O^{2\cdot-}$ compared to single L-arginine-loaded ACP hydrogels only. From 24h to 48h, the amount of $O^{2\cdot-}$ in the cell media containing AR10-ACP hydrogel or AR20-ACP hydrogel was maintained at around 14–15nM/h. To further define the importance of resveratrol in the depletion of superoxide anion production in bacterial endotoxin-stimulated macrophages cultured with the A-hydrogel, the analog of L-arginine (L-NAME)- known as NOS inhibitor [99] was added to the culture medium (**Fig. 4.6D**). We found that the treatment of RAW 264.7 cells with L- NAME resulted in incomparable changes in $O^{2\cdot-}$ formation in the case of LPS-stimulated cells, R-ACP hydrogels, or ACP hydrogels, except for the ACP hydrogel containing L-arginine. NOS inhibitors administered with A-ACP hydrogel did not affect $O^{2\cdot-}$ production within 24 h of incubation. However, after 48h of incubation, more than 22% of $O^{2\cdot-}$ production was blocked when NOS inhibitors were used along with A-ACP hydrogel. This result confirmed the problem of the utilization of L-arginine in wound healing[100]. Significantly, NOS inhibitors did not influence the concentration of $O^{2\cdot-}$ from AR-ACP hydrogel groups. The $O^{2\cdot-}$ production level was in the range of 14–15nM/h, similar to the levels shown with the non-inhibitor supplemented in the medium. The results suggested that adding resveratrol could help control the extracellular ROS induced by extracellular L-arginine availability in treatment.

4.3.4.3 Resveratrol helps to prolong the stability of nitric oxide generated from L-arginine in oxidative stress

Further, the cellular models of oxidative stress were established to support evidence about the synergy of L-arginine and resveratrol in the anti-oxidative process. The BMSC cells were treated with a strong oxidant (H_2O_2) for 24h to treat oxidative stress in BMSC cells (**Fig. 4.6E**). After subculturing established cells, $O^{2\cdot-}$ was overproduced in stress cells (p>0.05) (**Fig. 4.6F**). Consistent with DPPH results, the formation of $O^{2\cdot-}$ was gradually weakened compared to non-treated stress cells (p=0.0023). Like LPS-activating macrophage cells treated with A-ACP hydrogels, the intracellular $O^{2\cdot-}$ level was significantly increased in the oxidative stress cells (28.1±2.2 nM/h). The use of resveratrol and L-arginine in the combined therapy hydrogel had a prominent effect, similar to that of resveratrol single-loading hydrogels. The concentration of endogenous NO released from BMSC cells was

monitored (**Fig. 4.6G**). Despite evidence of the stimulation of resveratrol in response to endothelial NO synthase (eNOS)[101], the endogenous NO release from oxidative stress sBMSC treated with R-ACP hydrogel was comparable to that of non-treated cells or to bare ACP hydrogel. The nitric oxide (NO) level was only dominated in the cells culturing on the hydrogel with L-arginine. In the normal cell condition, NO was also strongly generated from the cells seeded on A-ACP or AR-ACP hydrogel surfaces (all $p<0.05$) compared to other types, revealing the function of arginine as a nitric oxide donor compound However, if NO is present nearby, the production of $O^{2\cdot-}$ could combine with NO to form peroxynitrite ($ONOO^-$) - a strong a short-lived oxidant that play a critical role for host defence[97,102]. The massive amount of ONOO- would delay the healing time, though, due to the prolonged inflammatory phage time [28]. Therefore, the fluorescent probe of peroxynitrite (DAX-J2 PON (Green)) was used to monitor the presentation of ONOO- in the cytoplasm of BMSC cells. For the normal BMSC cells, the signal of the peroxynitrite probe was absent in all treated samples (Fig. 4.6 H). However, in the oxidative stress cells, the green signal was detected inside the cytoplasm of almost all cells. The cell model cultured on native ACP form did not show a decrease in cell density with green fluorescent compared to non-treated. With the support of L-arginine, the ONOO- signals were strongly displayed, confirming the concern of L-arginine therapy. Interestingly, the green fluorescence was significantly dismissed upon treatment with hydrogels containing resveratrol. Only slight ONOO– generation was found for R-ACP hydrogels, which could be attributed to the reactions with endogenic NO or $O^{2-\cdot}$. Taking the example of resveratrol, despite the high amount of NO liberation from cells treated with AR-ACP hydrogel, intracellular ONOO generation was very small. In other words, the antioxidant capacity of resveratrol on suppressing intracellular ONOO- generation can help to maintain the NO concentration that would benefit angiogenesis and tissue repair during the wound healing process.
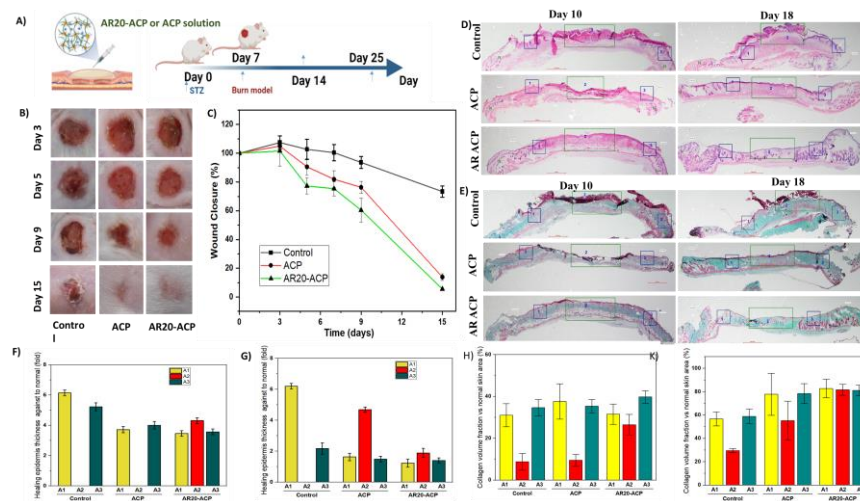
Figure 4.7: *A) In vivo burn wound healing on diabetic mice model. B) The photographs and (C) the statistical analysis of wound closure (n=3) of the burn wounds (100mm) at the given time. The evaluation of the re-epithelialization process of the diabetic wound. D) H&E staining images and E) MT staining images of diabetic wound tissues on the 10th and 18th day after different treatments, respectively. The rectangle indicated the wound edge (A1 and A3) and the center (A2) of the wound bed. Percentage epithelialization (n = 3) at day 10 (F) and day 18 (G) post-wounding are shown.*

4.3.5   Evaluation of the wound closure treated by hydrogel

The designed experiment is illustrated in the **Figure 4.7A**. Digital photographs of the wounds in each group are shown at different time points in **Figure 4.7B**, and the wound healing progress was determined by measuring the wound area over 14 days (**Fig. 4.7C**). The hydrogel-treated groups displayed extraordinary wound appearance. Wounds dressed with native ACP hydrogel were kept moist, leading to a bright color on the wound surface. The wound edge started the contracted process, and the average maximum wound area exhibited a

reduction of 14.43±2.35% compared to the 3rd day. AR20-ACP caused changes to both the speed and pattern of re-epithelialization, the healthy granulation tissue on the center of the wound, and the formation of scar in the wound edge, which was readily apparent on visual inspection at day 5. In addition, AR20-ACP hydrogel exhibited great accelerated wound closure with 77.23±5.23% remaining wound area.

4.3.6   *Evaluation of the regeneration of damaged skin treated by hydrogel*

On day 10, H&E staining (**Fig. 4.7D**) showed that the re-epithelialization was discernible within the wound edges (labeled A1 and A3) in the control groups. **Figure 4.7F** showed that the epidermal thickness of the advancing epithelial tongue was a 5–6-fold increase compared to the length of the epidermis in the typical skin region (labeled N). However, the center of the wound (labeled A2) in the control groups contained large necrotic and dermal cells. In addition, neutrophil infiltration, which is representative of severe allergic reactions and serious bleeding and other inflammatory cells, was observed in the wound area. Similar to controls, the administration of ACP hydrogel appeared to alter the regeneration process in the wound edges rather than that in the center of the wound, but with more incredible velocity. The change in epidermal thickness to the normal skin was smaller than in the control group (p=0.013). Also, the affiliated organs of the skin, such as hair follicles and sebaceous glands, appeared at the edge, which was missing in the control. Histological analysis indicated that only the animals treated with AR20-ACP hydrogel had fully restored the epidermis at all examined areas. The epithelial thickness was also comparable to wound edges or the wound center (all p>0.2). Further, the epidermis of the whole wound region was fully stratified, including terminally differentiated stratum corneum, through the vast majority of the wound surface. Together with epithelial coverage formation, neovascularisation is a crucial advantage of the AR20-ACP hydrogel. The density of newly formed blood vessels was 37.12 ±11.4% in the wound when AR20-ACP hydrogel was applied, nearly nine times higher than that of the native ACP hydrogel group. Specifically, the angiogenesis process was shown on most wounds with AR20-ACP but occurred only on the edges of the wounds treated with ACP hydrogel and was limited in the control groups.

By day 18, the restoration of wound skin structure was significantly different in three groups (**Fig. 4.7G**). The centers of control wounds with saline treatment had no epithelial coverage after 18 days. The re-modeling process in the edges wound was also unequal. The hemorrhaging and infiltration of inflammation cells appeared in A2 under the immature epidermis. In contrast, the full re-epithelialization of most wound-administered ACP hydrogel or AR20-ACP hydrogel was concluded by day 18. The significantly more effective re-modeling process was detected in the AR20-ACP hydrogel group. The epidermis thickness of wounds was comparable to that of undamaged skin. Notably, in the AR20-ACP hydrogel treatment, mice with complete wound closure also exhibited hair regrowth at the wound edges. Meanwhile, hair follicles and sebaceous glands were discerned in the dermal layer of wound centre, which was missing from other groups. These results demonstrated a well-organised wound healing process with AR20-ACP hydrogel.

To further clarify the advantages of AR20-ACP hydrogels in the diabetic wound healing process, Masson's trichrome-stained tissue sections of wounds with different treatments was set up (**Fig. 4.7D**). There was no significant difference in the organisation of the fibrous matrix in the dermal layer among the three groups in the wound-edge at day 10. However, in the wound centre, integrated collagen was observed only in the AR20-ACP group. The level of collagen deposition in AR20-ACP at day 10 reached 30–40% compared to undamaged skin (**Fig. 4.7H**). The denser and better arrangement, appearing as regularly organised bundles, was seen on day 18 in all experimental groups, especially for ordered collagen bundles in AR20-ACP hydrogel (**Fig. 4.7K**). Wounds with saline treatment displayed a higher cellular and vascularised granulation following the rapid increase in myofibroblasts compared to day 10, proposing the formation of scarring. However, the epidermis of these wounds did not completely close, which increased the risk of skin barrier dysfunction. With ACP hydrogels, the epidermis of the wound was re-generated; however, cellularity in the dermis was still high and increase scarring was a

possibility. As expected, the infiltration of cells in the dermal layer was absent. The collagen deposition in AR20-ACP-treated wounds showed a more fibrillar morphology in the dermal layer compared to the dense irregular collagenous connective tissue feature of the normal skin. Therefore, AR20-ACP hydrogels were validated with effectiveness in accelerating wound healing and skin regeneration in a diabetic mouse model. Moreover, in terms of inflammatory relief, granulation tissue formation, re-epithelialisation, remodelling and collagen deposition, the more rapid wound healing and more advanced skin regeneration over the whole healing process strongly demonstrated the efficacy and potential of AR20-ACP hydrogel in burn wound healing.

CHAPTER 5 DEVELOPEMNT OF THERMAL RESPONSIVE HYDROGEL FROM ALGINATE AND PLURONIC VIA CROSS-LINKING TECHNIQUE FOR BONE REGENERATION

5.1 Preparation of HNP BG

5.1.1 *Preparation of HNP nanoparticles*

Hemin first underwent a solvothermal carbonisation reaction in methanol to make HNPs. The TEM images show that the HNPs have a dispersive and uniform morphology (**Fig. 5.1A**). The DLS results showed that the average hydrodynamic diameter of HNPs was about 33.4 nm. However, the PDI value of HNPs indicated that the system had a highly polydispersed and moderately dispersed distribution. Encouragingly, a function of the delay time of HNPs in water is deconvoluted into a single exponential (**Fig. 5.1C**), confirming a single broad population. HNP solution (**Fig. 5.1D**) was clear and transparent after dissolving in water, confirming the highly dispersive property of HNPs. The ultraviolet–visible (UV–vis) spectrum of hemin in NaOH displays two split Soret bands at 360 and 385.5 nm and Q bands at 500 nm [115]. Under the carbonisation, the absorption peak of hemin was unchanged but showed a red-shift (Fig. 5.1E). It was observed that HNPs had another absorption peak at 266 nm, which was derived from the n–π* transition of the functional groups with a lone pair of electrons [218]. In addition, HNPs displayed fluorescent emission, whereas the raw material hemin had none, in agreement with some reports [115, 218]. Under UV light, the colour of the HNP solution changed from yellow to green (**Fig. 5.1D**). The fluorescent properties of HNPs were then examined in water. HNPs showed excitation-dependent emission features. As shown in **Fig. 5.1F** at the excitation wavelength of 470 nm, the HNPs showed a strong fluorescent emission at 500 nm, corresponding to the green colour, similar to previous reports. Based on these results, it can be deduced that hemin was carbonised by the solvothermal reaction and successfully produced hemin in the nanosized particles with a new physical property (fluorescent emission).

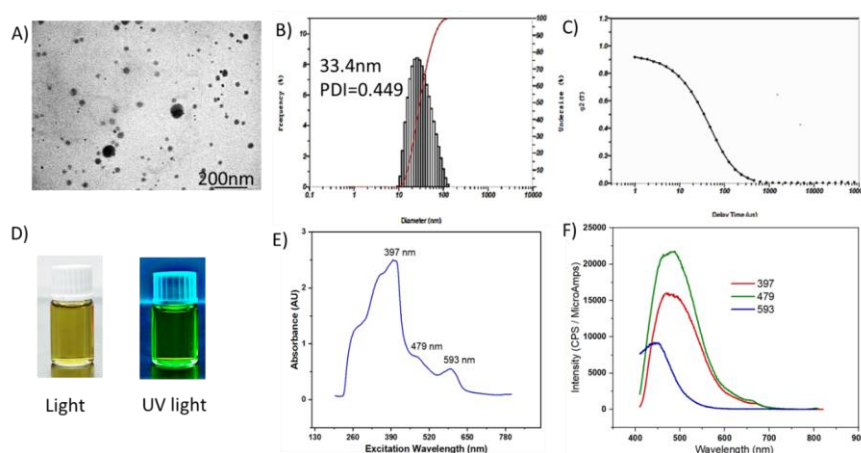**Figure 5.1***: Characterisation of HNPs. The typical TEM image (A), the hydrodynamic size in water (B) and the DLS autocorrelation functions (C) of the synthesised HNPs. (D) The photo image of vials containing HNP solution under white and UV light. The absorbance wavelength (E) and emission (Em) (F) spectra of HNPs in water at different excitation wavelengths.*
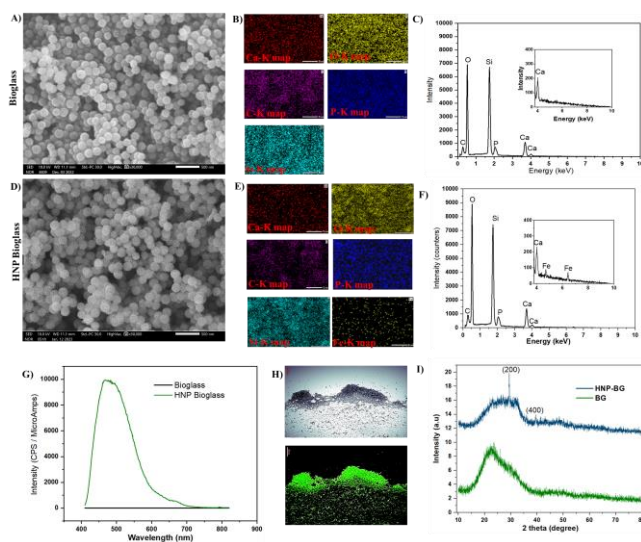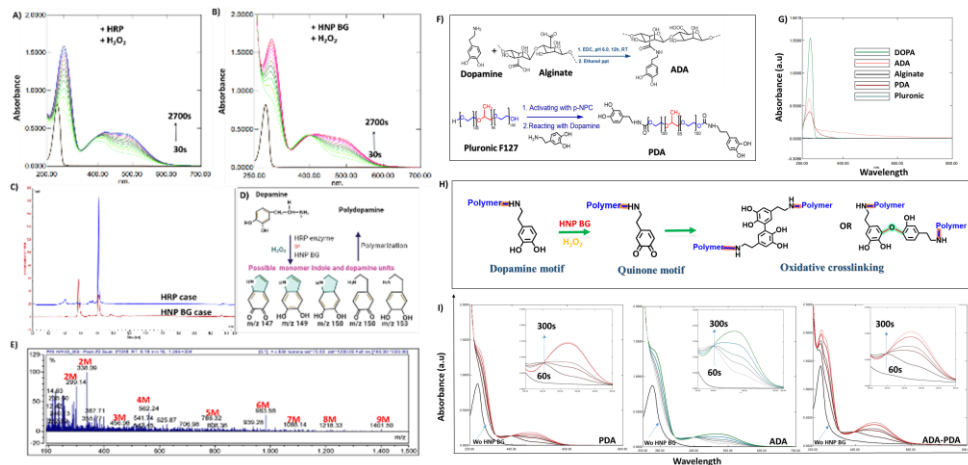
5.1.2 *Preparation of HNP BG*

Figure 5.2: *Characterisation of HNP BG. SEM image in combination with its surface mapping EDS for characteristic main elements (C, O, Ca, P, Si and Fe) of distribution and whole EDS of native bioglass BG (A, B, C) and HNP BG (D, E, F). (G) The emission (Em) spectra of HNP BG and BG nanoparticles in water at excitation 479 nm. (H) The figure of HNP BG under bright light and fluorescent light (Ex = 480, Em = 525). The XRD pattern of BG and its derivative HNP BG (I).*

The bioglass (BG) was synthesised via the sol–gel method. **Figure 5.2A** shows the size, morphology, and distribution using the SEM images and elemental analysis using the EDS spectrum of synthesised BG. BG was observed to be a size of around ~150 nm with dense, spherical, and monodispersed particles. According to the EDS mapping (**Fig. 5.2B, C**), the three main elements in BG, Si, Ca and P, are uniformly distributed in the BG. The addition of HNPs did not influence the size or morphology of BG (**Fig. 5.2D**). Compared to native BG, the EDS mapping (**Fig. 4.2E**), as well as the spectrum of HNP BG (**Fig. 5.2F**), displayed the new element signal corresponding to Fe, accounting for 0.77% by mass. Intriguingly, HNP BG showed a strong fluorescence emission at 500 nm when excited at 479 nm (**Fig. 5.2G**), similar to HNPs. Confocal microscopy was conducted to support this evidence (**Fig. 5.2H**). The green fluorescent signal was emitted from HNP BG under the excitation of λ = 480nm. The XRD patterns of native BG and HNP BG are compared in **Figure 5.2I**. As expected, the BG and HNP BG were approximately amorphous. However, some crystallisation had occurred in HNP BG. The identified crystalline phases were calcite (ICDD: 01-072-1937). In addition, the board diffraction peak in the XRD pattern of BG was a hypsochromic shift from the region of 20–25º to 23–32º, confirming the mixture of crystalline regions of hemin into a crystalline phase of BG [106,114]. According to the results obtained from the reported analysis, it can be concluded that the HNP BG was successfully synthesised in this study.

5.2 The potential of HNP BG as a catalyst for catechol crosslinking

Polymerisation process of DOPA was studied based on variations of UV–vis spectra in response to oxidation with H_2O_2 with the help of the HRP enzyme (**Fig. 5.3A**) or HNP BG (**Fig. 5.3B**). Inspected, HNP BG can catalyse the H_2O_2-driven oxidation of DOPA to aminochrome (AC), in analogy to HRP. Pristine DOPA exhibited characteristic peaks at 280 nm corresponding to the molecular electronic transition in phenolic catechol amines. The addition of H_2O_2 did not induce any change in the UV–vis spectrum of DOPA over 1 hour. Upon adding HRP or HNP BG, the peak at 280 nm immediately intensified and red-shifted to ~300 nm while a broad shoulder in the visible region (~400 nm) appeared, confirming the formation of different DOPA-derived quinones, as described in the literature [117,118]. With the increase of the incubation time, the absorbance due to the formation of the dopachromore intermediate DQ at 300 nm increased while the absorbance at 400 nm tended to broaden in the range of 400–600 nm, suggesting further transformation to the indole family.

Figure 5.3: *The oxidative pathway of DOPA under the catalyst of HRP enzyme or HNP BG in DI water. UV–vis spectrum of DOPA solution after addition of H₂O₂ and catalyst, HRP enzyme (A) and HNP BG (B) recording within 2700 s. The reaction was then analysed with LC−MS (ESI+) analysis (C). The suggested monomer forming after the oxidative reaction (D) was used to identify the self-polymerisation of the DA product under the catalyst of HNP BG (E). The function of HNP BG in performance of the crosslinking between catecholic polymers: F) The synthesis route of catecholic anchor (DA) polymers, alginate–dopamine (ADA) and Pluronic F127–dopamine (PDA) and (G) their UV–vis spectra along with precursor reactants (DOPA, sodium alginate and Pluronic F127); H)the real-time evolution of UV–vis spectra for PDA, ADA and the mixture ADA–PDA (1:1) solutions with the addition of HNP BG 5 mg/ml recording from 250 nm to 800 nm. K) The illustration of the formation crosslinking between dopamine motif on each polymer backbone.*

To confirm the UV–vis result, the behaviour of chromatographic retention and product ion spectra of oxidative DOPA were studied. Under the selected HPLC–MS analytical conditions, the peak retention time due to the reaction of DOPA and H_2O_2 under HNP BG was the same as the HRP enzyme (**Fig. 5.3C**), suggesting that the oxidation course of HNP BG is identical to the HRP enzyme. Further verifying the presence of the polydopamine structure, a rapid liquid chromatography/tandem mass spectrometry (LC–MS/MS) method has been developed. In fact, during the oxidative reaction, various monomers of polydopamine are generated. Oxidative coupling of DA units connecting two or more benzene rings by the formal loss of two hydrogen atoms is a well-known reaction for polydopamine. Based on the molecular weight of the possible building blocks proposed in **Figure 5.3D**, 5,6-indol-quinone (m/z 147) was selected as the monomer in this study, defined as M. Gratifyingly, the mass peaks could be detected for oligomers with different degrees of saturation from dimer to nonamer, as depicted in Figure 4E. The first one is the m/z dimer peak of 299.14 (2M + 6H) or 338.09 (2M + 6H + Ca^{2+}). The appearance of the peak at m/z 456.98 was assigned for the trimer oligomers (3M + 18). In addition, the tetramer (4M) was exhibited in the mass spectrum, which predicted the origin from the covalent bonding between trimer and pyrrolecarboxylic acid ($C_4H_{14}NO_3^+$) moieties derived from the oxidative degradation of indole units. Moreover, the positive spectra of the various polydopamine with higher repeating building block hybrids with calcium ions from HNP BG, such as pentamers (5M + 20 + Ca^{2+}), hexamer (6M + 30 + $2Ca^{2+}$), etc., were proposed in this study. Altogether, the results revealed the possible strategy of HNP BG as the alternative catalyst for DOPA crosslinking hydrogel.

5.3   Preparation of catechol precursor, catechol- alginate and catechol-pluronic

Figure 5.3F presents the fabrication process of these precursor polymers. The conjugation of catechol hydroxy phenols on the alginate backbone (ADA) was performed via the carbodiimide coupling reagent. In the case of Pluronic F127, the hydroxyl group at both terminal ends was first activated with p-nitrophenyl chloroformate to generate 4-nitrophenyl carbamates as a specific site for substitution of amino motifs on DOPA, resulting in the coupling of a catechol group to both ends of Pluronic F127 (ADA). Both native sodium alginate and

Pluronic did not show absorption bands in the range of 250–800 nm (**Fig. 5.3G**). After conjugating dopamine, UV–vis spectra of ADA and PDA show absorption bands at λmax = 280 nm corresponding to the L_a–L_b transitions in phenolic catecholamines in pristine DA. From UV–vis spectroscopy, Beer's law was used to calculate the amount of catecholic anchor on the polymer backbone. The conjugation efficiencies for alginate and Pluronic F127 were 13.91 ± 2.55% (30.7 ± 0.02 mg catechol/g alginate derivative) and 94.78 ± 3.22% (23.02 ± 0.78 mg catechol/g Pluronic derivative).

5.4   Preparation of the hydrogel from catechol-alginate and catechol-pluronic

5.4.1   *Examination of the formation of catechol crosslinking between two catechol precursors*

UV–vis spectroscopy was used to track the change in catecholic anchor polymers during reaction to investigate the gelation mechanism (**Fig 5.3 H**). The UV–vis results from the polymer-based DOPA solution samples in **Figure 5.3I** yielded conclusive results about the formation of catechol−catechol adducts between polymer-based DOPA triggered by H_2O_2 and HNP BG. For single DA derivative polymers, the quinone peak (λmax = 401 nm) appeared immediately after adding HNP BG, indicating the rapid oxidation of DOPA polymers in the presence of oxidants (Fig. 5.6C). Following that, the absorption peaks at 401 nm showed the bathochromic shift to 500 nm, possibly resulting from dicatechol formation, suggesting the formation of 5,5'-di(3,4-dihydroxyphenylalanine) (DOPA in dimer form) as the possible coupling mechanism through aryloxy radical formation on the DOPA phenyl ring (**Fig 5.3H**). These UV–vis profiles were matched precisely with the oxidation pristine DOPA shown in **Figure 5.3B**. Oxidation of dual DOPA derivatives showed results in the same spectra as a single derivative. However, the red-shifted quinone peak was quicker than that of the single one. Along with the main peaks comparing favourably with DA chrome, the peak at λmax = 300 nm was the emergence, which is believed to be a precursor to the formation of melanins, high molecular weight polymers crosslinked from catecholamines. The results described here indicate that dual DOPA derivative polymers, ADA and PDA, are capable of rapid gelation in situ under mild physical conditions.

5.4.2   *Preparation of the hydrogel*

Next, hydrogel formation based on DOPA derivative polymers in single or dual combination was studied via the sol–gel transition; the results are presented in **Figure 5.4A**. Consistent with previous reports showing the formation of DOPA derivative Pluronic F127 hydrogels, a higher concentration was required for hydrogel formation than that of the bare Pluronic. The addition of DOPA to the Pluronic F127 showed sol–gel transition properties significantly shift to the left with an increase to 40 %wt, whereas Pluronic F127 was ~16 %wt. It is known that the Pluronic copolymers aggregate with increasing temperature in the form of spherical micelles by enhanced hydrophobic interactions between PPO middle blocks of the copolymers. Above a critical concentration, the self-assembling Pluronic micelles are closely packed to generate a physically crosslinked hydrogel structure. The additional presence of a catechol group moiety at the PEO distal end of Pluronic F127 might disturb the well-ordered micellar integrity as well as the packing density due to the variation in hydrophilic/hydrophobic balance of Pluronic F127, thereby raising the gelation concentration [56]. With the addition of HNP BG along with H_2O_2, the gelation of PDA was shifted to a lower concentration regime. The gelation concentration of PDA was detected at 15 %wt at temperatures higher than 30 ºC. The gelation was reversible between 4 ºC and 30 ºC similar to the bare Pluronic hydrogel. This behavior was proved with the temperature sweep test. As shown in **Figure 5.4A,** 15% PDA the formulation was observed to regain its solution state, reaching almost the same start-up values of G' and G''. When HNP BG and H_2O_2 was added along PDA15, the viscoelastic response of PDA15 was significant changed. Upon heating from 5°C, only G'' was detected, confirming the liquid stage of sample. From 25ºC, the solution showed the ability to store energy elastically. After this point, G' is one order magnitude higher than G'', thereby inferring that gel structure formation. In addition, the colour of the PDA solution was changed from colourless to

dark brown, confirming the oxidative process of the catechol group [117-119]. HNP BG induced the oxidation of the DOPA motif and subsequent self-crosslinking between Pluronic micelles, which generated loops and tails on the shell layer of the packed Pluronic micelles, providing physically and chemically interconnected, tightly bound junctions between them. Therefore, the PDA_{15} with HNP BG/H_2O_2 indicated a predominant viscoelastic behavior typical of hydrogels while pure PDA_{15} was at typically observed for viscous solutions.
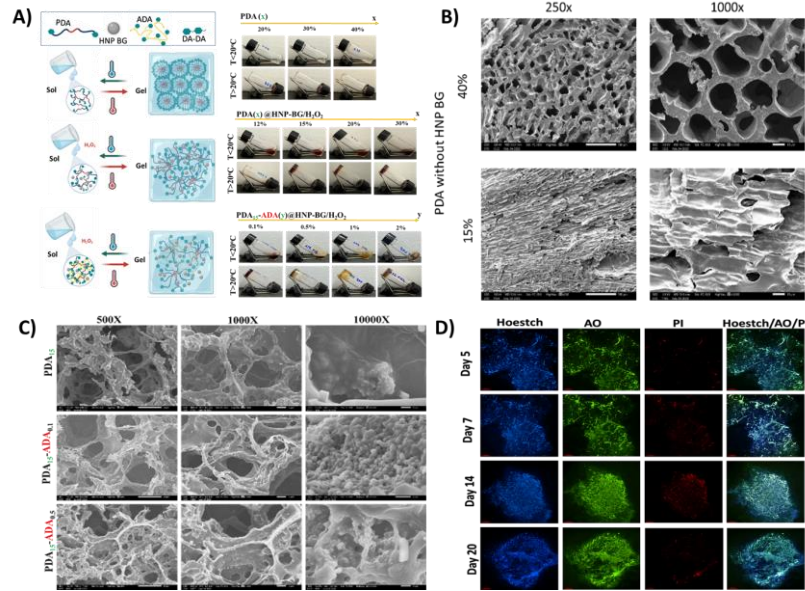
Figure 5.3: *A) Thermal responsive behavior of the resultant hydrogel. The tube inversion method for sol-gel conversion of PDA with/without HNP BG/H2O2 and the mixture PDA–ADA. x and y denote the concentrations of PDA and ADA, respectively. B) Morphology of PDA hydrogel without HNP BG at 40 %wt and 15 %wt. C) The morphology of the obtained hydrogel from PDA and the mixture between PDA and ADA with the help of HNP BG/ H2O2. D) The cytotoxicity of the resultant hydrogel: Live/dead staining of hMSCs laden with hydrogel was performed with Propidium Iodide (PI, red, dead cells), Acridine Orange (AO, green, live cells) and Hoechst 33342 (blue, cell nucleus).*

The mixture of 15%wt PDA and 0.1%wt ADA formed hydrogels within 60 s. The mixture of PDA–ADA maintained sol-like behaviour at cool conditions and returned to the gel stage at warm temperatures (T > 30 °C). Rheological study showed that G′ and G″ of PDA_{15}-$ADA_{0.1}$@HNP BG/H_2O_2 followed the function of temperature. The drastic change in elastic modulus and crossover between G′ and G″ at ca. 22.61 °C is characteristic for a sol–gel phase transition [120]. In contrast to PDA_{15}@HNP BG/H_2O_2, the elastic portion of the viscoelastic behavior appeared in the initial temperature testing condition, suggesting links inside the material, for example chemical bonds or physical-chemical interactions [121]. Increase the concentration of ADA to 0.5%, the sol-gel phase transition was unchanged (**Fig 5.4C**). However, the G'' values of PDA_{15}-$ADA_{0.1}$@HNP BG/H_2O_2 was higher than PDA_{15}-$ADA_{0.5}$@HNP BG/H_2O_2 after reaching the phase transition. This confirmed that the more interaction forces in PDA_{15}-$ADA_{0.5}$@HNP BG/H_2O_2 than that of PDA_{15}-$ADA_{0.1}$@HNP BG/H_2O_2. The existence of high density of crosslinking prevent the transformation of deformation energy into heat energy, suggesting the ideally elastic hydrogel [121]. However, at ADA concentrations at 1 wt%, we did not observe any significant sol–gel transition properties. In agreement to inverted tube method, the crossover between measured G′ and G″ curves of PDA_{15}-ADA_{1}@HNP BG/H_2O_2 were undetectable. Obviously, the G′ of this hydrogel was always higher than G″ at all temperature. Interestingly, increase the temperature, both G' and G'' were increased very obvious, indicating the sensitivity of this system to temperature. After 22-23°C, the viscosity of the composite system tends to be stable in the process of increasing the temperature. It was known that ADA alone became a gel state at 1%wt following the addition of HNP BG. This is not only the result of oxidative crosslinking of DOPA but also the result of the 'egg-

box' model of the alginate backbone with bivalent cations that release from BG [74,75]. Therefore, the higher the concentration of ADA, the density of crosslinking due to ADA is sufficient, and the disruption of micelles entanglement due to the PPO segment in PDA is offset; consequently, sol–gel transition due to temperature is eliminated.

5.4.3 Morphology of hydrogel

The morphology of resultant hydrogels was accessed by SEM technique using freeze-dried samples. The cross-section of PDA hydrogel at 40 %wt possessed a honeycomb-like structure with a relatively dense porous structure (**Figure 5.4B**). The pore size became larger with the reduction in PDA concentration to 15 %wt. This hydrogel demonstrated a tubular and reticular network morphology with lower interconnected pores within the hydrogel matrix, confirming the pseudo-gel stage.

In contrast, the introduction of chemical crosslinking in PDA 15 wt% under the catalytic activity of HNP BG (PDA_{15}@HNP BG/ H_2O_2) led to the spontaneous formation of a three-dimensional (3D) porous structure (Fig 5.3C). It indicated that the mechanism of crosslinking accompanied by reaction-induced phase separation leads to diverse morphologies of the resulting porous structure of crosslinked hydrogel [4,17,81,122]. When 0.1 %wt ADA solution was applied along with PDA 15 wt% (PDA_{15}-$ADA_{0.1}$@HNP BG/H_2O_2), the composite hydrogel showed a similar macroscopic structure as single PDA@HNP BG/H_2O_2, but with a high degree of interconnectivity. It was observed that the perfect miscibility was between these compositions as one phase with the absence of a separation zone. The increase in the concentration of ADA, a sponge-like network k structure, was observed in PDA_{15}-$ADA_{0.1}$@HNP BG/H_2O_2, but with relatively smaller pore size. Also, the walls of the micropores were much thicker, proposing a longer time for degradation. The highly interconnected structure in PDA_{15}-$ADA_{0.1}$@HNP BG/H_2O_2 hydrogel provides the necessary scaffold to retain tissue fluid and possess high oxygen and nutrient permeability[83,84,104]. Therefore, the design of hydrogels might be suitable for cell attachment and three-dimensional cell growth.

5.4.4 Evaluation of the injectability of hydrogel

Next, an evaluation was performed via rheology to ascertain if the hydrogels that were designed displayed the essential mechanical characteristics required for the creation of a clinically applicable drug delivery platform. Due to the sol-gel transition behavior, PDA15-ADA0.5@HNP BG/H_2O_2 could be injectable following the change in temperature. Frequency sweeps provide a relative ranking of elastic and viscous properties under constant strain. Increasing frequencies decrease relaxation times and favor elastic properties (G′, storage modulus) over viscous properties (G′′, loss modulus), as there is minimal time for energy to dissipate or for hydrogels to flow during testing[302]. These results indicate that the PDA15-ADA0.5@HNP BG/H_2O_2 has solid-like characteristics (e.g., G' greater than G'') over a broad range of frequencies when 37°C was applied (**Fig 5.5A**). In contrast, when PDA15-ADA0.5@HNP BG/H_2O_2 was at 20°C, no hydrogel was formed, and rheological characterization revealed that the mixture exhibited liquid-like properties. PDA15-ADA0.5@HNP BG/H_2O_2 hydrogel was easier to inject at the cool condition (T<20°C). Therefore, it is highly desirable to apply this scaffold at low temperatures. The injectability of the PDA15-ADA0.5@HNP BG/H_2O_2 sample at gel condition was also accessed. Analyzing the strain sweep at 37oC, it becomes evident that the hydrogel significantly reduces both storage and loss moduli beyond a specific yield strain, signifying material yielding (**Fig 5.5B**)[303]. When evaluating injectability using rheological data, the shear-thinning characteristic is first paramount [304]. As shown in **Figure 5.5C**, the viscosity of PDA15-ADA0.5@HNP BG/H_2O_2 hydrogel dropped approximately 7000 orders of magnitude as the shear rate increases from 0.1 to 200 (1/s), demonstrating that this material is extremely injectable[302, 305]. The strong decline in viscosity implies that the internal framework of the PDA15-ADA0.5@HNP BG/H_2O_2 network was disrupted under high-shear conditions. To regain its solid form after injection, the network structure would need to regenerate [306] spontaneously. To determine the ability of PDA15-ADA0.5@HNP BG/H_2O_2 to self-heal, the cyclic train time

sweep where material underwent multiple cycles of high and low strain conditions was applied. When applied strain at 200%, the G′ was lower than the G″, representing a gel-sol transformation behavior. The modulus of PDA15-ADA0.5@HNP BG/H_2O_2 rapidly and repeatedly restored to original levels once low strain condition (0.1%) was applied, confirming the rapid self-healing properties of this hydrogel (**Fig. 5.5D**). This also indicates the injectability of PDA15-ADA0.5@HNP BG/H_2O_2 at critical gel temperature [302].
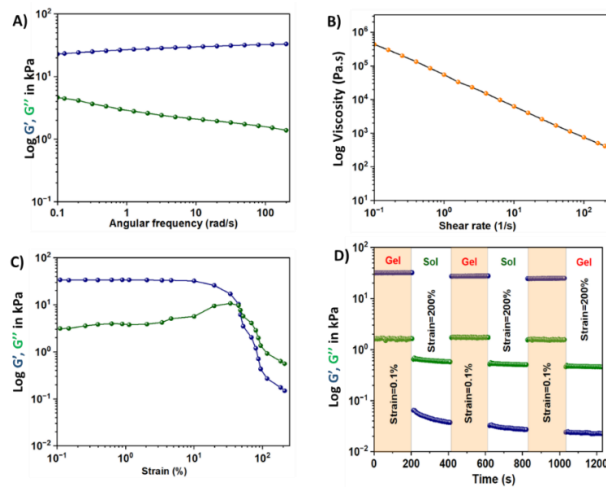

Figure 5.5: *PDA15-ADA0.5@HNP BG/H_2O_2 hydrogel exposes its rheological behavior that enables injection through needles. A) Oscillatory frequency rheology, B) Continuous flow, C) oscillatory amplitude rheology and cyclic train time sweep rheology for PDA15-ADA0.5@HNP BG/H_2O_2 at 37oC.*

5.4.5 *The cytotoxic of the resultant hydrogel*

The potential toxicity of the hydrogel needed to be tested. In 2D culture, the viability of hMSCs cultured with the extracted hydrogel solution was over 90% compared to non-treated cells at all culture times, indicating that the effect of the hydrogel degraded processes could be ignored. The potential toxicity of PDA$_{15}$-ADA$_{0.5}$@HNP BG/H_2O_2 was also tested with 3D culture. For this, hMSCs were laden in a hydrogel network, and a live–dead fluorescence assay was performed to observe and analyse the differences more intuitively. The live/dead staining images showed that most cells encapsulated in the tested hydrogels were viable (green) even at day 20 (**Fig. 5.4D**). However, some cells remained round after 5-day encapsulation. The number of spreading cells and their spreading extension increased with the incubation time. Finally, cells in the composite hydrogels developed into a typical spindle shape, in which pseudopods were clearly visible. Altogether, PDA$_{15}$-ADA$_{0.5}$@HNP BG/H_2O_2 displayed superior biocompatibility.

5.5 The potential of catechol hydrogel-based HNP BG for bone regeneration

5.5.1 *In vitro biomineralisation*

Bioactivity is one of the most important characteristics of the material for bone regeneration, which can be confirmed by monitoring the growth of hydroxycarbonate apatite (HCA) layers after immersing material in SBF for defined periods of time. The apatite-deposited surfaces with chemical compositions were observed by SEM–EDS analysis, as shown in **Figure 5.6**. Microscopic observations by SEM revealed that the PDA scaffolds' surface remained unchanged, depicting a relatively flat surface with a very low signal of Ca and P elements after 7 days of SBF immersion. After 14 days of mineralisation in SBF, the supersaturated ions in the SBF continued to precipitate on the surface of PDA. The EDS mapping suggested that the ratio of Ca/P on PDA was in the range of 0.42–0.6. However, from the XRD analysis, it was found that the deposited material on PDA was not apatite. In the case of hydrogel with HNP BG, the presence of HNP BG was observed on the surface of scaffolds with cauliflower-like structures. The surface was almost entirely covered by a large amount of small crystals when incubated for a longer time in SBF. Further, the EDS map proved that HNP derivative hydrogel surface composition was found to be Ca

and P elements with a higher Ca/P ratio over 2.0, predicting the presence of HA and another form of calcium, such as calcite. As per the reference from JCPDS no. 09-0432, the XRD pattern of hydrogel forming with HNP BG concluded that these precipitated crystals belonged to HA. It was also observed that the glass transformed into a nearly amorphous phase after 14 days of immersion. The glass had become more amorphous, and the HA peaks at $2\theta = 28.35°$ (1 0 2) and $2\theta = 39.8°$ (1 1 3) became sharper, indicating the formation of crystalline HCA. Along with the HCA signal, diffraction spectra of the HNP BG-driven hydrogel shown in **Figure 5.6 B-C** confirmed the appearance of calcite. However, the diffraction intensity of these peaks was higher in $\underline{PDA_{15}\text{-}ADA_{0.5}@HNP}$ $\underline{BG/H_2O_2}$ than in the single PDA hydrogel. Compared to native HNP BG, EDS mapping results showed that increased aggregation of Ca and P was observed on dual DA derivatives after 7 days of soaking, and these signals were identical to $PDA_{15}@HNP$ BG. The aggregation of the new Ca and P on PDA was observed on the surface of $PDA_{15}@HNP$ BG when the soaking time was extended to 14 days. In other words, ADA might help to increase the driving force of the crystallisation process resulting in an increase in biomineralisation. This is because alginate matrices contain carboxylate groups, which can interact with diffusing solutes such as Ca^{2+} from the SBF medium or the HNP BG, consequently increasing the supersaturation concerning the promotion of the nucleation of apatite or calcite structures on the surface of the PDA–ADA composite hydrogel in the early time as compared to HNP BG only [123,124]. Therefore, the bioactivity of $\underline{PDA_{15}\text{-}ADA_{0.5}@HNP\ BG/\ H_2O_2}$ was extensively higher than that of others.
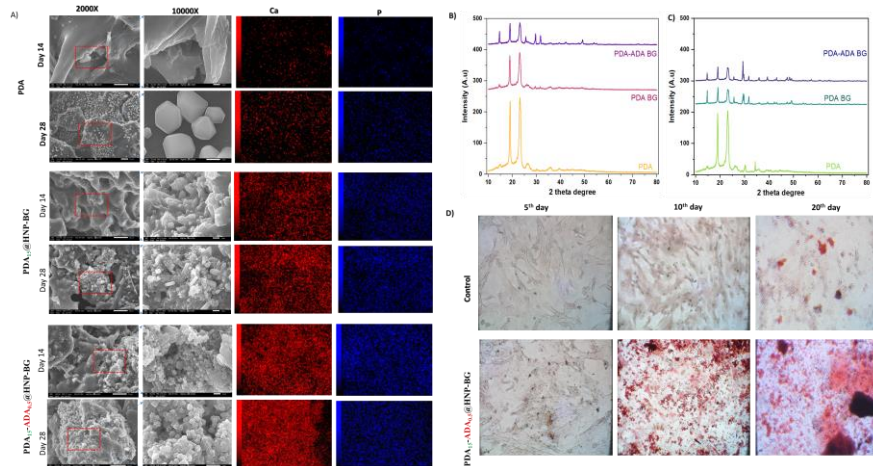

Figure 5.6: *In vitro biomineralisation promotive property of the design hydrogel. PDA, $PDA_{15}@HNP$ BG, $PDA_{15}\text{-}ADA_{0.5}@HNP$ BG). (A) The surface of this hydrogel at different magnifications (2000 X and 10.000 X) following the characteristic elements of Ca and P distribution and their corresponding EDS spectra (B); X-ray diffractometer patterns after 7 days (C) and 14 days (D) immersion in SBF at 37 °C.*

5.5.2 *Osteoinductive potential*

Bone mineralisation resulting from calcium deposition is known as a late marker in osteogenic differentiation. hMSCs were used to test whether $PDA_{15}\text{-}ADA_{0.5}@HNP$ BG/H_2O_2 induced osteogenic differentiation. Calcium mineralisation was detected via Alizarin Red S staining. As shown in **Figure 5.6**, calcium nodules were produced in the $PDA_{15}\text{-}ADA_{0.5}@HNP$ BG on day 7, while this phenomenon was lacking in the control hMSCs. The Alizarin Red staining of hMSCs cultured with hydrogel composite appeared more extensive at day 14 of differentiation, while the mineralisation of nearly the entire well was observed in the control (**Fig 5.6D**).

5.5.3 *Anti-bacteria*

As an effective material for combating infection and stabilising the chemical internal environment of bone defect sites, the antibacterial properties of the $PDA_{15}\text{-}ADA_{0.5}@HNP$ BG/ H_2O_2 hydrogel were also implemented in this study. The $PDA_{15}\text{-}ADA_{0.5}$ formed by the HRP enzyme and H_2O_2 was used for comparison purposes, defined as the control sample. *S. aureus* and *E. coli* were selected as models in this experiment. It was possible to verify that the $PDA_{15}\text{-}ADA_{0.5}$ hydrogel without HNP BG does not possess antimicrobial activity. The bacterium growth

increased in the first 24 h (10^9 CFU/mL, $p < 0.0001$), remaining stable at high bacterial concentrations during the rest of the assay period. When the bacterium was exposed to PDA_{15}-$ADA_{0.5}$@HNP BG/ H_2O_2 hydrogel, a remarkable decrease in the bacterium growth was detected. The hydrogel reduced the bacterial levels to lower than 10^2 CFU/mL, and $\geq$ 99% of *S. aureus* and *E. coli* were killed. Overall, the bacteria seem to be susceptible to HNP BG. It is well known that bioglass has intrinsic bacteria. The exchange of network-modifier ions in bioglass with hydrogen ions from the media causes an increase in pH and chaos in the osmotic pressure consequently inhibiting bacterial growth [46,49,112]. Therefore, PDA_{15}-ADA_3@HNP BG/ H_2O_2 hydrogels showed higher levels of antibacterial activity than the hydrogel formed with the HRP enzyme. Therefore, PDA_{15}-$ADA_{0.5}$@HNP BG/ H_2O_2 is an ideal material for bone regeneration applications.

CHAPTER 6   CONCLUDING REMARKS

6.1   Concluding remarks

This work developed injectable hydrogels comprising a thermally responsive polymer, Pluronic F127, and alginate using different methods with specific stiffness and specific biological cues for specific tissue regeneration.

- Successfully synthesized the thermal responsive hydrogel from the alginate derivative to pluronic via the grafted copolymer techniques, in detail:

+ Successfully prepared ACP hydrogel with thermal responsiveness to body temperature.

+ Successfully prepared the dual bioactive compounds (Resveratrol and L-arginine) loaded hydrogel, AR-ACP.

+ Successfully provided the practical status of the hydrogel on wound healing model in diabetic animal

- Successfully synthesized the thermal-responsive hydrogel from alginate and pluronic via the crosslinking technique, in detail:

+ Successfully prepared bioglass with peroxidase mimicking enzyme, HNP BG.

+Successfully prepared the hybrid hydrogel with temperature-responsive behavior, alginate, and pluronic using synthesized bioglass as a catalyst, ADA-PDA@HNP BG/ H_2O_2.

+ Successfully provided the status of the hydrogel on the ability in bone regeneration.

6.2   Future perspective

Despite the exciting outlook of the designed thermally responsive hydrogel, numerous tasks will require to commercialize in our daily lives. First, future research should focus on the scaling ability of the synthesis process to estimate the potential transferred techniques to the industry. In other words, the optimization process to increase the pilot of the study should be clarified. Second, the stability of the product should be approached to understand its storage condition and aging information. Although animals were used in this study, the mice's skin or mice's immunological systems are quite different from humans; large animals, such as dogs and pigs, … should be used in the future. In addition, the hydrogel showed the best adaptation to cells. This provides evidence for applying cell-laden hydrogels, which will be further studied to provide information on their application in the multifunctional tissue engineering field. For example, further research should be considered with tissue regeneration with personalized medicine using cell therapy combined with the designed scaffold. Furthermore, the standardized criteria for evaluating these hydrogels should be conducted to bring the product to clinical trials.

LIST OF THE PUBLICATIONS RELATED TO THE DISSERTATION

1. **Le Hang Dang**, Phuong Doan, Tran Thi Yen Nhi, Dinh Trung Nguyen, Bich Tram Nguyen, Thi Phuong Nguyen, and Ngoc Quyen Tran. "Multifunctional injectable Pluronic-cystamine-alginate-based hydrogel as a novel cellular delivery system towards tissue regeneration." International Journal of Biological Macromolecules 185 (2021): 592-603.

2. Vo Le, Tuong Van, Ngoc Quyen Tran, **Dang Le Hang**, Thanh Tuyen Nguyen, Quynh Anh Bui, Nguyen Dinh Trung, Nguyen Dat Thinh et al. "Impacting different structures of injectable Pluronic-conjugated alginate (chitosan) hydrogels on their physicochemical characteristics and morphological fibroblast behavior." International Journal of Polymer Analysis and Characterization 27, no. 3 (2022): 205-219.

3. **Le Hang Dang**, Hong Tuoi Do, Kim Tram Pham, Phuong Thu Ha, Thi Phuong Nguyen, Tan Phat Dao, Ngoc Quyen Tran. "Injectable thermogel incorporating reactive oxygen species scavenger and nitric oxide donor to accelerate the healing process of diabetic wounds". International Journal of Pharmaceutics 648 (2023): 123576.

4. **Le Hang Dang,** Vu Nhu Quynh, Thuy Tien Nguyen, Thi Hong Tuoi Do, Thi Kim Tram Pham, and Ngoc Quyen Tran. "Thermally-responsive and reduced glutathione-sensitive folate-targeted nanocarrier based on alginate and pluronic F127 for on-demand release of methotrexate." International Journal of Biological Macromolecules 263 (2024): 130227.

5. **Đặng Thị Lệ Hằng,** Trần Ngọc Quyển, National Patent (VN 1-2021-01465): QUY TRÌNH TỔNG HỢP HYDROGEL NHẠY NHIỆT TỪ VẬT LIỆU ALGINAT-CYS-PLURONIC, cấp năm 2024.

Other related publications

1. **Le Hang Dang**, Thai Tuan Tran, Minh Tuan Nguyen, Thao- Han Luong, Dat Thinh Nguyen, Minh-Dung Truong, Phuong Le, Hai Khoa Le, Thuy-Tien Dang, Ngoc Quyen Tran. "Syringeable hydrogel based β-cyclodextrin and mixed micelles for Methotrexate delivery". Journal of Drug Delivery Science and Technology, 92 (2023), 105299.